Description of manuscript changes

General changes

Throughout the manuscript, several sentences were altered to increase readability and address some concerns pointed out by reviewer #1. Several changes were made to the manuscript after the replies to reviewer #1 were made, thus, the provided replies are not necessarily up to date. A better description and differentiation of the different Pt100 strings was made. References to the different periods of data acquisition were strengthened. There are now clear indications in the image captions as to whether there was any smoothing of data. The introduction was reorganized to provide a proper introduction to cloud chambers, their importance and the specific importance of temperature measurements for new particle formation (NPF) experiments and cloud formation experiments. The laboratory calibration of sensors was also altered to clarify several points which were less understandable

Specific changes

Introduction

Three paragraphs were introduced. Firstly, highlighting the scientific relevance of tank reactors in the study of atmospheric processes and NPF, along with the contributions of the CLOUD chamber to these studies. Secondly, highlighting the importance of expansion chambers in the study of in-cloud processes as well as the contributions of the CLOUD chamber to this particular field of study. Thirdly a motivation on the importance of temperature measurement and stability in the study of NPF and in-cloud processes.

NEW - Chamber operation

A second section was added to describe the general operation of the CLOUD chamber, both during NPF studies and in-cloud process studies.

Thermal system

A third section now goes into specific detail on the thermal control system and temperature sensors available in CLOUD. Figure 1 was updated to include the

position of the trace gas input lines. Table 1 was updated to include an estimate of the position of the calibration Pt100 sensor strings.

Results - NPF and in-cloud process experiments

The sections on the results obtained during NPF and in-cloud process experiments were largely altered to increase readability, a table was added describe the different NPF experiments used to acquire data.

Appendix A

Annex A was altered, mostly to increase readability.

Editor replies - 02 Nov 2017

References to the supplementary material were added to the manuscript.

Replies to reviewer #1

The replies to reviewer #1 have been largely kept the same as the ones provided in the interactive discussion on the AMT website. Some replies were edited to reflect the current status of the manuscript. As some of the paragraphs that were said to have been placed either suffered changes or were removed in favor of readability

Major Questions

Question 1: After reading the manuscript several times, now have the impression that during the calibration campaign only runs with steady flow conditions have been performed. Is this true? If so, why did you not perform evacuations for cloud formation as well? How much data (e.g. in hours, or if evacuations how many) did you take during the calibration campaign. How many hours did you measure in flow conditions during the data campaign? I think this information would be useful and should be added to the manuscript. Please clarify! In general, more information about the experiments performed during both campaigns might be helpful, maybe summarize the experiments in a table?

The calibration campaign stated in the manuscript did indeed only consist of measurements taken during steady state conditions. No evacuations were preformed. The reason for the calibration campaign was to create a calibration curve for the different permanent temperature strings that exist in CLOUD (the Pt100, TC and OS strings). In order to do this, several points at different operational temperatures in CLOUD are required. One temperature measurement is thus required to be acquired at stable conditions. Although expansions (evacuations) provide important information about the dynamics of the chamber, they do not provide information relevant to obtaining a calibration curve of the sensors. Each temperature point taken during the calibration campaign took 24 hours. During data campaigns the permanent sensor strings (Pt100, TC, OS) were constantly turned on and acquiring data. The relevant nucleation experiments used were taken during separate periods between 29th of September and 29th of October 2014. Each temperature point during data campaigns consists of a period no smaller than 3 hours. The manuscript has been altered to better relay this information and the focus of these experiments and a table containing the major relevant parameters of these nucleation experiments has been included.

Question 2: Why Pt100 sensors were chosen for the calibration strings? This is not motivated in the manuscript. However, as you state, they have a rather long response time (180 s), which seems insufficient for cloud experiments, where temperature drops much faster than this? How do you compare temperatures from the fast response sensors to these slow response sensors? Please explain!

The manuscript was indeed confusing regarding this point. A distinction must be made between the permanent Pt100 string and the calibration PT100 strings (PTH and PTV). The description of the Pt100 string and more specifically the 180s response time was regarding the permanent Pt100 string. The calibration Pt100 strings use a completely different hardware and software construction, allowing for 1s time resolution measurements and smaller time response.

Question 3: Why do you average the data over 15sec? Does it make sense in case of the Pt100 with time constants around 180sec? On the other hand, 15secs smooth out fluctuations in the fast sensors responses. Do you also smooth data during evacuations?

The data in the plots shown in figures 3 and 4 was altered using a median filter. This filter applies a median to a specified window of data (in this case 15 seconds) as opposed to the averaging mechanism suggested by the reviewer that applies an average instead. The reason for this data alteration is two-fold. First, to remove any outliers from the measurement of the distribution of temperature. Secondly to provide the reader with an easier to read figure, since without the filter, the reader would not be able to see the fluctuations of the data and the different signals shown. Indeed, temperature drops during cloud formation experiments (expansions) were at times much faster than 180 seconds. The temperature measurements shown in this manuscript for expansions, however, do not show measurements from the permanent Pt100 string, only the fast response OS and TC strings. The permanent Pt100 string only exists to measure nucleation experiments, the comparison of data from this string to the fast response sensors is thus valid, taking into account the total run time of nucleation experiments (several hours). The data for expansions was not altered since we were not measuring a constant temperature distribution but a time-changing one. In every instance where data was altered, it is explained to the reader in the manuscript.

Question 4: I would like to see a schematic of CLOUD chamber that shows more detail, e.g. the "serpentine" pipe (page 3, line 71), regulation and gate valves (line 51), sampling ports for cloud measurements. Particularly the valve positions in respect to the temperature sensors would be good to know!

The gas input pipes are located below the lower mixing fan, which is then responsible for pulling the inputted gas and mixing it with the air inside the chamber. They insert the gases at a height of a couple of centimeters above the

bottom of the chamber (-150 cm < z <-140 cm using figure1) Figure 1 has been altered to include a representation of the gas input valves along with a representation of the axis used to calculate the sensor positions in the chamber. The reader can now estimate the position of the pipes in relation to the temperature sensors (using figure 1 and table 1).

Question 5: A large part of the introduction (i.e. from line 28) reads more like a potential chapter 2 "chamber operation" (or similar). I would expect more introduction about cloud chambers and the importance of temperature measurements, temperature stability e.g. what motivates your manuscript.

The manuscript has been changed to reflect the expressed views. Section 2 is now named chamber operation and part of the offending text in the introduction was moved there. The introduction was increased to include the relevance of cloud chambers in the study of NPF and in-cloud processes, CLOUD's contribution to these studies and the specific importance of temperature measurements in the CLOUD chamber.

Calibration Runs

Question 1: Are calibration and data runs performed at the same relative humidity? (Think of cloud formation, latent heat release...)

No dedicated measurement of relative humidity was taken during the calibration runs. However, the proximity of the calibration sensors to the TC and OS sensors as well as the sheer length of measurements during the calibration campaign drastically reduces the uncertainty caused by varied values of relative humidity. The campaign data was also taken at various relative humidity values. The nucleation experiments were a part of scheduled experiments of one of the many institutes that are a part of the CLOUD consortium and were not subject to any change. There were no dedicated experiments during the data campaign for temperature measurements (either nucleation or expansion experiments). The manuscript has been altered to reflect this concern.

Question 2: Are there calibration runs that were performed at data run like flow rate? You could simply let the instruments suck as well – higher flow rate might increase the temperature instability. Thus, it would be necessary to show. How are clouds formed in a calibration run? If clouds are only formed in expansions, what is the meaning of calibration runs for cloud studies in the chamber?

The instruments referred to in the manuscript and this question were not yet present at the time in CLOUD. The instruments present in CLOUD data campaigns are the property of several institutes in the CLOUD consortium (and outside it as well). These instruments are taking measurements at several sites around the world during the year. Only at specific times are they present at

CLOUD. At the time of the calibration campaign, no instrument had yet arrived. The very high cleanliness standards of CLOUD also prevent us from keeping instrument ports open for large periods of time. Thus it was simply impossible to mimic the flow conditions of CLOUD data campaigns without inadvertently increasing the pressure in the chamber. No clouds were formed in the calibration run. As stated in the first question, the goal of the calibration campaign was to provide a calibration curve for the temperature sensors. No other instruments were calibrated during this campaign. The manuscript was altered to clarify the definition of the calibration campaign throughout the text.

Question 3: You only show examples of the measurements in the figures for the calibration campaign. Is there a way of showing all data in one plot? Are there any expansions made during the calibration campaign? As the calibration strings were only installed during the calibration campaign, this would need to mimic conditions as they would be during a measurement campaign. If not, what is the aim of the calibration campaign?

Figure 3a, 6a, 6b, 7 and 10 show data taken during CLOUD data campaigns. If the reviewer is referring to the measurement distributions provided in figure 4, this can be remedied. It would however, require the reviewers clarification. No expansions were made during the calibration campaign as explained in the first and previous question. See previous question for reason of calibration campaign

Question 4: You state e.g. in line 148 that around 300 expansions have been performed in the latter campaign. I would expect something like scatterplots showing all data and median/average values (if necessary grouped into classes by speed of expansions to show all data. "Various experimental conditions" are mentioned in the abstract, not mentioned any further later on! What are these various conditions? They could be used to group data for plots. Where is the statistical analysis? What about significances?

Over 300 expansions were indeed preformed in the CLOUD campaign. An indirect representation of the distribution of expansions is presented in figure 9 accompanied with statistical analysis. The temperature change in an expansion is indirectly related to the time of the expansion. The variation of experimental parameters is too large to provide an easy visualization of the parameters. Presenting the different expansions also goes outside the scope of the manuscript, as only the relevant dynamic behavior of expansions in the CLOUD chamber is studied in this manuscript. A statistical analysis is provided with the use of the expansion reheating parameters in figures 9 and 8. The reheating parameter in our opinion provides a quantitative parameter to analyze individual expansions.

Lab Calibration

Question 1: You mention that the WIKA reference thermometer is calibrated in the temperature range 0-100∘C. How to you use it at temperatures below

freezing? What confidence do you have in its performance there?

The WIKA thermometer was only used for the positive temperature values, including the 0ºC point. The appendix has been edited to clarify this point.

Question 2: You mention liquid nitrogen as calibration point for cold temperatures. Is it valid to assume linear calibration between -196.21∘C and 0∘C, why? How did you get calibration points at temperatures between -70∘C and 0∘C, i.e. at temperatures that would potentially be used for experiments in the chamber? (E.g. you could add one point by using salt/ice mix and one point by using dry ice in a Dewar flask).

As expressed in the manuscript, the Pt100 sensors were calibrated using the Callendar-van Dusen equation. This equation provides a curve for resistance of Pt100 sensors in the range of temperature of [-200 ºC,600 ºC]. This equation is a quadratic equation for temperatures above 0º C and a third degree equation for temperatures lower than 0 ºC. This relationship is based on the properties of platinum that are part of the sensors. There were no laboratory temperature points in the range of CLOUD's negative temperatures especially because the reference thermometer was not absolutely calibrated below 0º C. The Callendar-van Dusen equation along with the estimated parameters will provide a relationship between each sensor's resistance and temperature in the whole range of CLOUD operating temperatures. The uncertainty of the measurements of the Pt100 sensors was estimated on a worst case scenario using the Monte Carlo study for the ranges of temperatures in CLOUD (including the negative temperatures). The manuscript was altered to clarify first the use of the Callendar-van Dusen equation and secondly the importance of the Monte Carlo study in the calculation of the temperature uncertainty for points without laboratory measurements.
The suggested salt-water mixture suggested by the author was considered but the use of said mixture in the laboratory would go against the strict cleanliness standards of the CLOUD experiment, running the risk of contaminating further campaigns after placing the strings in the chamber. The manuscript was altered to clarify this point:

Question 3: How did you calibrate at 0 ∘C, this is not mentioned in the text? Figure A2 is showing a very different behaviour of the sensors at 0∘C compared to the water bath calibration points (which, as you state, start at 2∘C). So, how trustworthy is the point at 0∘C?

The calibration at 0ºC was accomplished by using a mixture of milipore water and ice. During this phase transition it is guaranteed that the temperature is at 0ºC. There are, however some concerns to take into account, mostly related to the volume of the Huber unit used. The most important of which is the possible existence of convection currents that increase the uncertainty of the measurement. The manuscript was altered to clarify this point.

Question 4: Why are the OS, TC and Pt strings not calibrated directly in the lab as well? How exactly is linear interpolation performed for the Pt string (page 8, line 237/238)? Elaborate!

The reason for the creation of these specialized strings was to make an in-situ calibration of the permanent temperature sensors. It was noticed that when the sensors of the permanent strings were disconnected from their readouts, their calibrations changed. This makes it impossible to disconnect the strings from the chamber and make a proper calibration only to reconnect the readouts and find out that the calibration had changed. These specialized strings were made in such a way that the string could be unmounted and mounted in the chamber while keeping the individual sensors connected to their respective readouts, allowing for a laboratory calibration and subsequent in-situ chamber calibration. The manuscript now stresses this point throughout with passages such as the following which has been added to the end of section 2 to clarify this point:

"Removing the OS, TC and PT sensor strings for calibration would require disconnection from their readout electronics, which can result in a shift of their calibration."

In response to the concern as to how the interpolation of the sensor was made. This was a spatial linear interpolation of the temperature between the position of PTH sensors and the permanent Pt100 sensors. The following text was added to the manuscript as an effort to explain how the interpolation was made for the also non working PTH2 (see question 4 in next section), which also applies for the permanent Pt100 string and this has been stressed in the manuscript:

"PTH2 was non responsive after being placed in the chamber. Thus its measurement was replaced by a spatial linear fit between the measurements of PTH1 and PTH3 defined by::

$$T^*_{PTH2} = T_{PTH1} + (r_{PTH2} - r_{PTH1}) \frac{T_{PTH3} - T_{PTH1}}{r_{PTH3} - r_{PTH1}} \quad (1)$$

where r_{PTHi} and T_{PTHi} are, respectively, the radial position and temperature measured by the PTH sensor of index i, as defined in Table 1.

Other questions - which were not answered in other sections

Question 1: "experimental hall temperature" – wall temperature?

This indeed refers to the hall temperature at CERN where the CLOUD chamber is placed. Since it is a large hall shared by many other experiments, not to mention provides access to all scientists in and out of CLOUD to (verify instrumentation, etc..), it is simply impossible to provide temperature control for this hall at CLOUD operational temperatures). The feed-through gas pipes

travel a short path (a few meters) through this hall before going either through the temperature controlled serpentine cable or being directly sent into CLOUD and there is an inevitable alteration of temperature during this path.

Question 2: Appendix: This describes the calibration in detail. Isn't the temperature calibration a main point in this study?

This question was also considered by the authors. The decision was to provide an appendix to the paper due to the fact that the manuscript is related to the analysis of the temperature stability, uniformity of the chamber. While the calibration of the sensors and how it was done is indeed important to show, it should not overshadow the end goal of the manuscript.

Question 3: Figure 4: How did you choose which sensors you show here? Motivate your choice. You could also show all other sensors in a supplement.

The sensors were chosen as they are the sensors at the middle of each respective string. A supplement has been prepared with the measurements of all other sensors in the string at the respective temperature, containing the requested plots, which are shown at the end of this document.

Question 4: Figure A4: You mention a malfunction of the PTH2 sensor, was this true for the whole campaign?

This was indeed true during the whole calibration campaign. This was resolved in data analysis by creating a virtual sensor via a spatial linear interpolation of the temperature between the radial position of PT1H (145 cm) and PT3H (90 cm) much as the same used for calibrating the permanent Pt100 string. An explanation of the interpolation mechanism can be found in question 4 of the previous section and as that question states, the manuscript has been updated.

Question 5: Were the OS4 and OS5 sensors replaced ater the calibration campaign (as obviously they showed an unusual behaviour)?

The sensors were not replaced, as doing so would involve removing all other sensors from their respective readouts. This has been clarified in the manuscript.

Question 6: Table 1: From this table one could think that the TC and PTH / OS and PTV sensors have the same position. It would be better to indicate the offset in the table, eg. by saying "0 (-20)" in the Height column (TC and PTH), and accordingly for the radius column for the OS and PTV sensors.

The sensors were placed in their strings and installed in the CLOUD chamber in an effort to place them in the closest possible position to each sensor to be calibrated. No measurement was made to determine the offset, visual inspection

concluded that the sensors were offset by no more than 1 cm. As suggested the values PT $\pm$ 1 cm were added to the PTH and PTV sensor positions in table 1 to indicate that their positions did not exactly match.

Question 7: Table A4: Why are PT4 and PT6 missing?

The permanent Pt100 string is only a 5 sensor string. PT4 was not functioning at the time of the calibration campaign and data campaign. This malfunction occurred during one of many efforts to calibrate said string in lab. One of such efforts must have damaged the sensing tip. During these efforts we noticed the shift in calibration when reconnecting the electronics which led us to make the calibration process described in the manuscript. The manuscript has been altered to address this concern.

We again would like to thank the reviewer for the time taken to appraise this manuscript. We hope that these replies along with the provided supplemented material and changes to the manuscript can provide a more favorable recommendation.

Replies to reviewer #2

We would firstly like to thank the reviewer for the favorable appreciation of the manuscript. Below we address the requests brought forth by the reviewer. They follow the requested format by AMT. Reviewer requests are in green followed by the author's response.

Request 1: It may be necessary to illustrate one or two examples of scientific studies one could do with such high precision measurement in the CERN CLOUD chamber.

The manuscript was kept somewhat vague in regards to preformed experiments in order to focus on the quality and implications of the preformed measures. Several examples of studies preformed at CLOUD which require very accurate temperature control have been added to the introduction section.

Request 2: The authors have mentioned in the text the importance of precise temperature measurements but a concrete example of an experiment that has been carried out in the CLOUD chamber will be more convincing to the readers.

Two factors are weighted in the decision to not include specific experiment details. Firstly, we would like to stress the need to not bog the user down in experimental details that do not concern temperature measurements. Secondly, in every CLOUD campaign, several experiments are performed every year, such that, while some similarities exist, experiments are performed by different institutes and operators. As stated in the previous answer, several examples of different experiments preformed in CLOUD are now provided in the introduction section for the more curious readers.

Replies - 02 Nov 2017

In order to comply with the comments on the Editor's report, which suggested a link be added in the manuscript, connecting the supplementary material, we have altered the manuscript text in the following ways:

1. On line 152-153, the following sentence was added:
   "Supplemetary material provides distribution of residuals for all other sensors."

2. The caption of figure 4 was also altered to contain the following sentence:
   "See supplement material for distributions of other sensors."

Manuscript prepared for Atmos. Meas. Tech.
with version 2015/04/24 7.83 Copernicus papers of the LaTeX class copernicus.cls.
Date: 2 November 2017

Temperature uniformity in the CERN CLOUD chamber

António Dias[1], Sebastian Ehrhart[1,a], Alexander Vogel[1,b], Christina Williamson[2,c], João Almeida[1,2], Jasper Kirkby[1,2], Serge Mathot[1], Samuel Mumford[1,d], and Antti Onnela[1]

[1]CERN, CH-1211 Geneva, Switzerland
[2]Goethe University Frankfurt, Institute for Atmospheric and Environmental Sciences, 60438 Frankfurt am Main, Germany
[a]Now at Max Planck Institute for Chemistry Atmospheric Chemistry Department Hahn-Meitner-Weg 1, 55128 Mainz, Germany
[b]Now at Paul Scherrer Institute, Aarebrücke, 5232 Villigen, Switzerland
[c]Now at Chemical Sciences Division, NOAA Earth System Research Laboratory, Boulder, CO and CIRES, University of Colorado, Boulder, CO
[d]Now at Kapitulink Lab, 476 Lomita Mall, Stanford University, Stanford, CA 94305-4045

Correspondence to: António Dias (amcbd89@gmail.com)

Abstract. The CLOUD (Cosmics Leaving OUtdoor Droplets) experiment at CERN is studying the nucleation and growth of aerosol particles under atmospheric conditions, and their activation into cloud droplets. A key feature of the CLOUD experiment is precise control of the experimental parameters. Temperature uniformity and stability in the chamber are important since many of the processes under study are sensitive to temperature and also to contaminants that can be released from the stainless steel walls by upward temperature fluctuations. The air enclosed within the ~~3 m~~26 m^3 CLOUD chamber is equipped with several arrays ("strings") of high precision, fast-response thermometers to measure its temperature. Here we present a study of the air temperature uniformity inside the CLOUD chamber under various experimental conditions. Measurements were performed under calibration conditions and run conditions, which are distinguished by the flow rate of fresh air and trace gases entering the chamber: 20 l/min and up to 210 l/min, respectively. During steady-state calibration runs between -70 °C and +20 °C, the air temperature uniformity is better than ±0.06 °C in the radial direction and ±0.1 °C in the vertical direction. Larger non-uniformities are present during experimental runs, depending on the temperature control of the make-up air and trace gases (since some trace gases require elevated temperatures until injection into the chamber). The temperature stability ~~varies~~ is ±0.04 °C over periods of several hours during either calibration or steady-state run conditions. During rapid adiabatic expansions to activate cloud droplets and ice particles, the chamber walls are up to 10 °C warmer than the enclosed air. This results in ~~non-uniformities~~ temperature differences of ±1.5 °C in the vertical direction and ±1 °C in the horizontal direction while the air returns to its equilibrium temperature with time constant of about 200 s.

1 Introduction

The Intergovernmental Panel on Climate Change (IPCC) considers that the largest source of uncertainty in anthropogenic radiative forcing of the climate is due to increased aerosol since pre-industrial times, and its effect on clouds (Myhre et al., 2013). Most of the increased aerosol has resulted from anthropogenic precursor vapours that, after oxidation in the atmosphere, can form particles which may then grow to become new cloud condensation nuclei (CCN). By current estimates, ~~about~~ more than half of all CCN originate from nucleation rather than being emitted directly into the atmosphere ~~(Merikanto et al., 2009),~~ (Gordon et al., 2017), but the vapours and mechanisms responsible remain relatively poorly known.

~~A solution for studying the previously refered processes is the use of experimental chambers inside which a thorough control of all important parameters is ensured (Paulsen et al., 2005; Zink, 2002). Temperature is an important parameter in atmospheric process estimation (Gordon et al., 2016). Maintaining temperature stability and uniformity in these chamber measurements ensures that the chemical reaction rates in the chamber do no fluctuate either in time or in space (Maahs, 1983). Accurate measurement of temperature is also necessary to measure the onset of ice formation in chamber experiments (Riechers et al., 2013; Connolly et al., 2012)~~Laboratory experiments for studying atmospheric processes such as new particle formation (NPF) under controlled conditions have generally used tank or flow reactors. Raes and Janssens (1986) used a flow reactor made of glass to study ion-induced nucleation at 22 °C. A similar setup was used by Ball et al. (1999) to study nucleation of sulfuric acid, water and ammonia. Large teflon chambers provide lower loss rates to the walls and allow correspondingly longer residence times, making it feasible to grow aerosol particles to larger sizes and at lower vapour concentrations (Cocker et al., 2001).

The CLOUD experiment at CERN ~~(Kirkby et al., 2011; Duplissy et al., 2016)~~ (Kirkby et al., 2011) has achieved sufficient suppression of contaminants (Schnitzhofer et al., 2014) inside a large, 3 m diameter stainless steel chamber to allow controlled ~~aerosol nucleation, growth and~~ NPF and cloud activation experiments to be performed ~~in the laboratory under atmospheric conditions . The chamber is~~ over the full range of tropospheric temperatures and trace gas concentrations. CLOUD has presented a series of measurements of atmospheric particle formation rates for different chemical systems. Theoretical considerations and early measurements (Lovejoy, 2004) indicated a strong temperature dependence for the nucleation rates of sulfuric acid particles. This has been confirmed by CLOUD in, for example, Kirkby et al. (2011) and Kürten et al. (2016).

Expansion chambers are used to study in-cloud processes such as the homogeneous freezing of super-cooled liquid droplets (Möhler et al., 2003) or cloud droplet chemistry (Jurányi et al., 2009). These experiments require the formation of cloud droplets or ice particles on CCN in the chamber. Clouds can be formed in the CLOUD chamber by adiabatic expansion and cooling of humid air. This allows cloud microphysics and aqueous-phase chemistry to be studied in the CLOUD chamber, for

example, phase transitions of cloud particles (Nichman et al. (2016)), or aqueous phase oxidation of SO_2 in cloud droplets (Hoyle et al. (2016)).

To understand new particle formation rates in the troposphere and lower stratosphere requires measurements at their ambient temperatures. Moreover, experimental NPF studies require stable temperatures over periods of several hours and a near-homogeneous temperature distribution over a large-volume experimental vessel. In the case of cloud formation by adiabatic expansions, fast-response and accurate temperature sensors are required to measure quantities such as the homogeneous freezing temperature or the onset of cloud droplets and their later evaporation. Here we present a study of the temperature uniformity and accuracy achieved in the CLOUD chamber under a) ideal conditions (with no deliberate additional heat) and b) operational conditions (where additional heat is introduced into the chamber by UV light and warm gases).

2 Chamber operation

The CLOUD chamber is a 26 m^3 cylindrical stainless steel vessel which is filled with humidified artificial air ~~to which ozone and selected trace vapours is added~~and chosen trace atmospheric vapours such as O_3 or SO_2. The ion concentrations inside the chamber can be precisely controlled over the full tropospheric range with a pion beam from the CERN Proton Synchrotron(Suller and Petit-Jean-Genaz, 1995). To ensure adequate mixing of the ~~27 m^3 stainless steel~~ chamber, two large mixing fans operate ~~on~~ at the top and bottom of the chamber~~(Voigtlander et al., 2012). In order to truly evaluate the reliability of the chamber, several studies must be carried out. The following presents the result of a thorough temperature study of the CLOUD chamber carried out during two separate campaigns in 2014.~~ , respectively (Voigtlander et al., 2012).

3 ~~Chamber operation~~

The CLOUD chamber normally operates at 5 mbar above atmospheric pressure (the small excess ensures that no contaminant vapours enter the chamber through the sampling ports). However, ~~the chamber can also be operated in a classical Wilson cloud chamber mode to create liquid or ice clouds (Wilson and Wilson, 1935). During this operation,~~ for cloud formation experiments, the air in the chamber ~~at high relative humidity (>90% RH)~~ is first raised to about 220 ~~-~~mbar above atmospheric pressure and ~~then allowed to reach thermal equilibrium. When equilibrium is reached~~a high relative humidity (>90% RH) is established. When thermal equilibrium is re-established, the pressure in the chamber exhaust pipe is reduced to 65 mbar below atmospheric with a high-volume blower, and then the ~~main~~ air inlet valve ~~for~~ to the chamber is closed. A controlled adiabatic pressure reduction is then performed back down to 5 mbar overpressure, which progressively cools the air and forms a liquid or ice cloud when the RH ~~in the chamber~~ rises above 100%. The pressure reduction is controlled with two regulation valves and two gate valves, which provide a selectable

and highly flexible pressure profile lasting between 10 s and 10 minutes. The low exhaust pressure (-65 mbar) ensures sufficient pressure difference to drive the expansion down to a final 5 mbar chamber overpressure. Once the chamber reaches 5 mbar, the main air valve is re-opened to maintain ~~that pressure~~the small over-pressure. During the expansion a cloud is maintained in the chamber and experiments are performed on cloud processing of aerosols, ice nucleation, and the effects of charge on cloud microphysics. The cycle can be repeated up to three or more times with a single CCN population, so the effects of multiple cloud processing of aerosol can be studied.

3 CLOUD thermal system

As well as precise control of ~~trace precursor vapours~~precursor trace gases, UV intensity, ions, relative humidity and pressure, it is important to maintain good temperature uniformity and stability in the CLOUD chamber since many of the processes under study are sensitive to temperature, and contaminants can be released from the walls by positive temperature fluctuations~~(Duplissy et al., 2010).~~ . Temperature control is achieved by enclosing the chamber in a thermal housing through which air circulates at a precisely-controlled temperature between -70 °C and +100 °C. The 100 °C temperature is used for bakeout cleaning of the chamber walls between experimental campaigns. Figure 1 shows a schematic of the CLOUD thermal system and its components.

Here we present a study of the air temperature uniformity inside the CLOUD chamber during ~~a campaign solely aimed at temperature sensor calibration, late~~ two campaigns. The first, in July 2014, ~~and the~~ was dedicated to calibration of the temperature sensors and evaluation of the thermal non-uniformities in the chamber under ideal conditions (no additional heat sources). The second was the CLOUD9 data campaign, September–November 2014. In addition, we calibrated a set of Pt100 calibration strings (PTH and PTV, see below) in the laboratory ~~during early July 2014.~~ prior to the calibration campaign. Concerning the present paper, the two CLOUD campaigns are distinguished by the flow rate of fresh air and trace gases entering the chamber: 20 l/min and 210 l/min, respectively. ~~The high~~ CLOUD9 involved experiments to produce secondary organic aerosol particles, as well as expansions to form clouds. The high air plus trace gas inlet flow rate during the data campaign is required to compensate for the ~~sampling flows of analyzing~~ air continuously extracted by analysing instruments attached to the chamber. During both campaigns, the main air supply passes through a 10 m heat exchanger ("serpentine") pipe inside the CLOUD thermal housing (see below) to bring its temperature close to that of the chamber air before injection. However, during measurement campaigns, some trace gases are injected warm into the chamber at flow rates of around 1 l/min each, which ~~can influence~~ influences the temperature uniformity inside the chamber. ~~All trace~~ Trace gases are injected ~~vertically from~~ individually at the bottom of the CLOUD chamber, ~~mixing of gases is ensured by the two mixing fans on the top and bottom of the chamber.~~ close to the main air

inlet and just below the lower mixing fan. Only O_3 is mixed with the inlet air before entering the serpentine pipe heat exchanger to avoid localised high concentrations of O_3 in the chamber.

~~The CLOUD chamber is enclosed in a thermal housing designed to maintain a highly uniform and stable air temperature inside the chamber at any value between -70°C and +100°C. CLOUD data campaign experiments are performed at temperatures below 30°C; cleaning of the chamber walls by bakeout of contaminants is performed at 100°C (Kirkby et al., 2011; Duplissy et al., 2016; Kupc et al., 2011). Figure 1 shows a schematic of the CLOUD thermal system and its components.~~

The temperature of the air inside the CLOUD chamber is measured by several precision thermometer strings: a) two horizontal strings oriented radially near the mid plane of the chamber~~that use either~~ , one using platinum resistance thermometers (Pt100, denoted PT)~~or thermocouples~~ , the other using thermocouple sensors (TC) and b) one vertical string that uses GaAs optical sensors (OS). The Pt100 sensors are four-wire sensors, with National Instruments (National Instruments Corp.) NI 9217 readout electronics. Figure 2 shows some details of the TC and OS strings. The thermocouple sensors are type K, with National Instruments (National Instruments Corp.) NI 9214 readout electronics. GaAs optical sensors (OTG-F with Pico-M single channel readout; Opsens Inc.) are used for the vertical temperature string since ~~the existence of~~ a high electrical field ~~to clear out ions rules out~~ of up to 20kV/m in the chamber—to remove ions—rules out the use of conventional thermometer sensors with electrical wires. The thermocouple and optical sensors have a low mass (0.5 mm diameter sensor tip with 75 μm stainless steel wall thickness and 30 mm free length) and a fast response time: 3 s ($1/e$) in air. However~~the horizontal~~ , the Pt100 sensors have a higher mass (1.5 mm diameter stainless steel sheath with 100 μm wall thickness) and slower response time (180 s in air). ~~The positions~~ Table 1 provides the positions in the CLOUD chamber of the temperature sensors of ~~all~~ the five strings (TC/PTH, OS/PTV and PT)~~in the CLOUD chamber are summarized in Table 1~~.

~~The thermal non-uniformities~~ Temperature differences over the large volume of the CLOUD chamber ~~span several orders of magnitude depending on the preformed experiment~~ under steady run conditions are small and require precise (~0.01 °C) calibration of the temperature sensors. ~~The~~ Removing the OS, TC and ~~Pt100 strings present in the CLOUD chamber are connected to specialized data readouts. Removing the sensor strings to calibrate requires that the sensors be disconnected from their respective electronics, this results~~ PT sensor strings for calibration would require disconnection from their readout electronics, which can result in a shift of ~~the previous calibration. It is thus impossible to remove the strings for calibration and place them back in the chamber using the same calibration.~~ their calibration. We therefore constructed dedicated horizontal and vertical ~~Pt100~~ calibration strings (PTH and PTV, respectively) in which each Pt100 sensor had been calibrated in close proximity to a certified WIKA (WIKA Alexander Wiegand SE & Co. KG) Pt100 reference thermometer, which itself was calibrated to ~~to 0.03~~$\pm$0.03 °C absolute precision. ~~These sensors , unlike the Pt100 string already present in the CLOUD chamber and despite also being~~ The sensors

of PTH and PTV are four-wire ~~sensors~~ Pt100 thermometers, with National Instruments NI 9217 ~~readout electronics,~~ readouts. These sensors do not have the same high mass of the ~~first sensors~~ Pt100 sensors installed on the PT sensor string, allowing for ~~fast responses equal~~ faster responses similar to the TC and OS sensors. After laboratory calibration, the PTH and PTV calibration strings were then mounted in the CLOUD chamber alongside the TC and OS strings, respectively, to transfer ~~the calibrations . The Pt100~~ their calibrations *in situ*. The calibration strings, PTH and PTV, ~~are~~ were only installed during the temperature sensor calibration campaign, when no electric field~~and instruments are~~ , no humidity and no trace gases were present. The calibration ~~procedure~~ procedures (both in ~~laboratory and in-situ) is~~ the laboratory and *in situ*) are described in detail in Appendix A. All the measurements presented in the following analysis correspond to calibrated sensor temperatures.

4 Temperature uniformity during calibration and ~~nucleation~~ NPF experiments

Figure 3 shows typical examples of the time series of thermometer sensors during ~~experimental~~ NPF runs and calibration periods. When the experimental conditions are not adjusted, the temperatures of individual sensors show drifts of only a few 0.01 °C over periods of several hours. ~~Despite these temperature sensors being active for the whole CLOUD campaign, the most useful nucleation experiments found to characterize the chamber were sections of day-long experiments consisting of particle creation via nucleation and subsequent expansion once the sizes of the particles reached relevant values. The nucleation part of these experiments was the focus of these measurements. The period of nucleation was in all cases over 3 hours, during which no changes were made to the experiments. Table 2 summarizes the most relevant parameters of the experiments.~~ Table 2 summarises the experiments selected to characterise the chamber temperature uniformity during the CLOUD 9 campaign.

Figure 4 shows the temperature residuals of individual sensors from their mean values, after slow trends in the data have been removed. The standard deviations of Gaussian fits to the data are 0.012 °C, 0.018 °C, and 0.004 °C for the TC, OS and PT strings, respectively. Comparison of the TC and PT residuals shows that short term (<15 s) fluctuations of the air temperature in the CLOUD chamber are very small (<0.01 °C). Furthermore, the comparably small OS residuals show that these sensors are in principle capable of ~~below 0.05~~around 0.02 °C measurement precision. Supplemetary material provides distribution of residuals for all other string temperature sensors.

Figure 5 shows representative temperature non-uniformities measured by several sensor strings in the radial and vertical directions during calibration runs at 21 °C and 1 °C, respectively. For these data, the temperature non-uniformity (maximum difference from the mean for the entire string) measured by the Pt100 calibration strings is ±0.01 °C in the radial direction and ±0.04 °C in the vertical direction. Comparison with the other strings shows close agreement of the TC string (panel

a) but somewhat larger residuals for the OS string (panel b), reflecting larger systematic errors in the OS calibration.

Figure 6 shows the temperature non-uniformity in the horizontal and vertical directions at chamber temperatures between -70 °C and 20 °C during ~~both~~ calibration runs (filled circles and diamonds) and steady conditions during data campaigns (hollow triangles). The temperature non-uniformity is ~~characterized~~ characterised as the maximum temperature difference of any sensor from the string mean, Max ΔT. A clear trend is seen in all temperature strings ~~for~~ of increasing non-uniformity as the chamber temperatures is lowered, which results from an increased temperature difference between the chamber and the ~~non temperature controlled~~ CERN experimental hall (around 20 °C). Nevertheless, under ideal (calibration) conditions the temperature uniformity ~~lies below~~ is better than $\pm$0.06 °C in the radial direction and $\pm$0.1 °C in the vertical direction, for chamber temperatures between -70 °C and +20 °C. During experimental campaigns, there is a high flow of fresh make-up air and trace gases (210 l/min) which can lead to higher non-uniformities in the vertical direction of up to $\pm$0.5 °C (green triangle symbols in panel b), depending on the temperature control of the make-up air. However, even during experimental campaigns, the radial temperature uniformity is ~~lower~~ better than $\pm$0.06 °C. Different ~~values of~~ fan speeds (up or down hollow triangles) do not ~~seem to have any influence in~~ show any influence on the temperature homogeneity.

5 Temperature characteristics during cloud formation experiments

Following an adiabatic pressure reduction, the temperature of the air in the chamber is below that of the walls. The wall temperature is essentially unaffected by the adiabatic cooling since its mass is several hundred times greater than the enclosed air mass. Therefore the walls transfer heat into the air and eventually bring it back into equilibrium at its original temperature, before the pressure reduction took place. ~~This warming rate can thus be used to characterize an expansion. The operation of the chamber can be evaluated by behavior of the warming rate for different parameters~~The rate of warming is a characteristic of the chamber surface area and volume, and determines how long a cloud can be maintained in the chamber before it evaporates. The rate of warming of the air can be described by a Newton's cooling law (Incropera and DeWitt, 2007):

$$\frac{\partial T}{\partial t} = -\frac{A\mu}{C}T = -\lambda T,$$

where A is the area of the chamber, μ is the heat transfer coefficient between the walls and the air, and C is the heat capacity of the air. These constants are absorbed into a single reheating rate coefficient, λ, that ~~characterizes~~ characterises the CLOUD chamber. The ~~characteristic reheating rate~~

reheating rate coefficient can be obtained by fitting the temperature versus time with an exponential curve given by

$$T(t) = T_w + (T_0 - T_w)e^{-\lambda t}, \quad (1)$$

where T_w is the wall temperature and T_0 is the initial temperature at $t = 0$, immediately after the adiabatic pressure reduction has finished. The ~~characteristic~~ reheating time constant ~~τ can be found by calculating $1/\lambda\tau = 1/\lambda$~~.

Around 300 adiabatic expansion ~~(pressure reduction) experiments~~ experiments to form clouds were performed during CLOUD9~~, September–November 2014. All were analysed and combined to improve the statistical precision of the results~~. Figure 7 shows ~~an exampleof an adiabatic expansion to form a cloud in the CLOUD chamber~~one example. The pressure reduction takes place over a period of 5 minutes, after which the temperature returns to its equilibrium value over the next 30 minutes. The red line shows an exponential fit to the reheating period (Eq. 1) with a time constant, $\tau = 200$ s. Figure 8 shows ~~the distribution of reheating rate calculated by each sensor for all expansions made. The figure also shows that withing experimental uncertainty the rate of reheating~~ that the air reheating rate is the same everywhere in the chamber ~~. This is expected for a well-mixed chamber.~~ and is the same for a wide range of experimental conditions. Figure 9 shows that λ ~~as a function of~~ depends only weakly the initial temperature reduction, ΔT. ~~It also shows that λ is only weakly dependent ΔT. The slight dependence on ΔT probably results from the increased importance of relatively warm make-up air at high ΔT.~~

During adiabatic expansions, air temperatures are up to 10 °C cooler than the walls, so large thermal non-uniformities may be anticipated. In Fig. 10 we show an example of the temperatures measured with vertical and horizontal strings during and after a fast (80~~seconds~~ s) adiabatic pressure reduction at -30 °C. Compared with operation under equilibrium conditions (Fig.~~10), much~~ 6), larger non-uniformities of up to ~~around $\pm$1.0~~1.5 °C are present ~~at the minimum temperatureafter an adiabatic expansion, in both radial and vertical directions (turbulence during an expansion ensures complete~~ while the chamber returns to its equilibrium temperature. Turbulence during the expansion ensures efficient mixing of the chamber ~~)~~during the expansion, so the initial temperature non-uniformities are similar in the vertical and horizontal directions. Thermal non-uniformities in the radial direction subsequently decrease as the air reheats and approaches the wall temperature. However, non-uniformities in the vertical direction reach a maximum around 2 minutes after the end of the expansion ~~. The vertical string shows clear evidence of~~ due to thermal stratification as the ~~chamber~~ air reheats, with warmer air ~~flowing~~ convecting to the upper part in the chamber (Fig. 10c). The radial string shows the effect of relatively warm make-up air entering the chamber after the expansion has finished and the main air inlet valve has been re-opened to maintain the baseline chamber pressure at +5 mbar. This can be seen in Fig. 6d by the higher temperatures of TC5 and TC6, which are closest to

the axis of the chamber and mixing fans. The flow of relatively warm make-up air partly contributes to the vertical stratification since the air exhaust pipes are located at the top of the chamber.

6 Conclusions

In order to ~~characterize~~ characterise the temperature uniformity of the air inside the CERN CLOUD chamber, we have constructed and calibrated several thermometer strings using various sensors (Pt100, thermocouple and optical/GaAs). Our measurements show that, under stable calibration conditions, the temperature uniformity is better than $\pm$0.06 °C in the radial direction and $\pm$0.1 °C in the vertical direction, for chamber temperatures between -70 °C and +20 °C. This excellent performance for a large-volume (26.1 m^3) chamber underscores the quality of the CLOUD thermal control system and thermal housing. Moreover, during periods when the experimental conditions are not adjusted, the chamber air drifts by only a few 0.01 °C. During ~~data taking~~experiments, there is a high flow of fresh make-up air and trace gases—up to around 210 l/min—to compensate for the air extracted into sampling instruments. This can lead to higher thermal non-uniformities unless the make-up air is carefully adjusted to match the chamber temperature before injection. Larger non-uniformities of up to ~~around~~ ~~$\pm$1.0~~1.5 °C occur during adiabatic expansions to form clouds in the chamber, since the walls are up to 10 °C warmer than the enclosed air. After an adiabatic expansion, the chamber air is reheated by the walls and returns to its equilibrium temperature with a time constant of around 200 s.

Appendix A: Thermometer sensor calibrations

Calibration of the horizontal and vertical Pt100 calibration strings

Careful calibration of all thermometer sensors used in the CLOUD chamber is required to extract meaningful results from the thermal measurements. Two ~~temporary~~ calibration Pt100 strings were specially constructed to allow in-situ calibration of the permanent CLOUD temperature sensors (TC, OS and PT). One vertical string (PTV) ~~focused on calibrating~~ was used to calibrate the vertical OS string and one horizontal ~~focused on calibrating~~ string (PTH) to calibrate the horizontal TC and ~~Pt100~~ PT strings. Pt100 sensors were used ~~for these~~ in the PTH and PTV strings due to their ~~proven~~ precision, reliability, temperature range and ~~calibration process~~well-defined calibration procedure. Calibration of the sensors ~~in the horizontal and vertical Pt100~~ on the PTV and PTH calibration strings (PTH and PTV, respectively) was carried in the laboratory in ~~early~~ July 2014. After ~~calibration and assembly~~ assembly and calibration of the PTH and PTV strings, they were mounted in the chamber alongside the TC, PT and OS strings, ~~respectively,~~ and then used to calibrate the latter ~~two~~ strings *in situ*, as described below.

The ~~Pt100~~ calibration strings are designed to allow the sensors to be ~~dismounted~~ detached from the string without ~~disconnecting~~ disconnection from their readout electronics (Fig. A1). The wiring from the sensors to the readout electronics passes through the support tube for the string. The cables have sufficient length to allow the sensors to be detached and brought together. In this way the ~~Pt100~~ sensors can be placed in close proximity with a reference Pt100 during inter-calibration in water baths or liquid nitrogen, ~~and the calibrations cannot be affected by disconnecting and reconnecting~~ without disconnection from their readout electronics. A certified WIKA (WIKA Alexander Wiegand SE & Co. KG) Pt100 reference ~~thermometer–calibrated~~ thermometer—calibrated according to ISO standard IEC751—was used as the absolute reference to calibrate the individual PTH and PTV sensors. The WIKA Pt100 reference thermometer is calibrated to 0.03 °C absolute ~~systematic~~ temperature uncertainty in the range 0–100 °C.

The PTH and PTV sensors were calibrated according to the Calendar-Van Dusen (CVD) equation Callendar (1887); Dusen (1925), which relates the resistance, R (Ω) and temperature, T (°C) of ~~platinum resistance thermometers by:~~ a platinum resistance thermometer by:

$$R(T) = \begin{cases} R_0 \left[1 + A\,T + B\,T^2\right] & \text{if } T \geq 0 \\ R_0 \left[1 + A\,T + B\,T^2 + (T-100)\,C\,T^3\right] & \text{if } T < 0 \end{cases} \tag{A1}$$

The standard values for a Pt100 sensor are as follows: $R_0 = 100\,\Omega$, $A = 3.908 \times 10^{-3}\ \Omega\ °C^{-1}$, $B = -5.775 \times 10^{-7}\ \Omega\ °C^{-2}$ and $C = -4.183 \times 10^{-12}\ \Omega\ °C^{-3}$ Commission et al. (2008). We determined fitted values of these parameters for each ~~of our Pt100 sensors in our~~ sensor in the calibration procedure, as described below.

All calibration string ~~Pt100~~ sensors were wired through their respective strings and connected to their readout electronics. The sensors were then placed in close proximity ~~in a millipore water bath along~~ with the reference ~~Pt100 thermometer~~ WIKA thermometer in a water bath, ensuring no contact was made between sensors. ~~In order to comply with CLOUD~~The water bath was filled with ultrapure water from the CLOUD humification system. CLOUD's cleanliness standards ~~,~~ do not allow the use of organic solvents or brine as thermostat liquid, and so only pure water and liquid nitrogen were ~~allowed~~ available for the laboratory calibration~~of the Pt100 sensors. A comprehensive statistical~~ . A Monte Carlo analysis of the calibration was made in order to ensure the calibration provided an acceptable measurement uncertainty at temperatures inside the whole range of measurements made in CLOUD (see below).

The Huber CC-K15 liquid bath (Huber Kältemaschinenbau AG) controlled the water temperature to better than 0.02 °C stability over the calibration range from 2 °C to 70 °C. A 0 °C point was obtained using a ~~millipore water bath containing ice, ensuring~~ mixture of CLOUD ultrapure water and ice. The WIKA reference thermometer confirmed that the temperature was ~~at 0°C while ice was present in the bath~~ °C. For calibration at lower temperatures, the sensors and reference ~~Pt100~~ WIKA sensor were placed in a dewar flask filled with liquid nitrogen. An electrical barometer was used to

measure the atmospheric pressure. The temperature measured at the boiling point of liquid nitrogen agreed within 0.01 ~~ºC~~ °C with standard value for nitrogen at the measured atmospheric pressure ~~, however, for callibration purposes, the calculated value at atmospheric pressure was used via a standard atmospheric pressure reader~~ (-196.21±0.0096 ~~º~~ °C at 966±1 mbar). For the calibration we used the standard value of the liquid nitrogen boiling point at the measured atmospheric pressure.

A least squares fit of Eq. A1 was then applied to the calibrated temperature measurements for each ~~Pt100~~ sensor. The C parameter was fixed at the standard value since it was poorly constrained by the calibration points. Moreover, propagation of the uncertainties showed that uncertainties in B have a larger effect than uncertainties in C. The residuals of the fit are shown in Fig. A2, and the fitted parameters and errors and uncertainties are ~~summarized~~ summarised in Table A1.

~~In order to ensure that calibration uncertainties were acceptable at temperatures in the range of CLOUD chamber experiments (no negative points used in the calibration),~~ We used a Monte Carlo method ~~was performed to evaluate the temperature uncertainties of the Pt100 sensors according to the uncertainty in the fitted CVD parameters. A sample of 1000 of fit parameters were chosen for each sensorat a given temperature from their respective values and errors (assuming a normal distribution of the fit parameters), and the resistances were calculated. The resistances were then converted into temperatures. The standard deviation of these temperature distributions were then taken to be the measurement error at that temperature. This was repeated at various temperatures over the range from~~ to verify that, after applying the CVD fits, the uncertainties in the calibration string sensors were negligible. From table A1, each sensor's estimated parameters were used to create a lookup table between resistance (R) and temperature (T) for the range -70 °C to ~~+~~70 ~~°C. The results are summarized in Fig.~~ C (a range spanning all of the current CLOUD measurements), using equation A1. The same estimated parameters were then assumed to follow a normal distribution of values around its fitted value, with a standard deviation equal to its uncertainty. From those distributions a set of 1000 trios of R_0^{fit}, A^{fit} and B^{fit} were retrieved. Using each trio, a similar lookup table was created using A1. Using both lookup tables, the temperature at the same resistance value was compared for all 1000 trios. The average temperature difference represents the uncertainty introduced in the measurements by fitting the Calendar-Van Dusen coefficients. These differences are plotted in figure A3 and show that~~almost all Pt100~~ , after applying the CVD fits, almost all calibration sensors have an uncertainty below 0.01 °C over the full ~~temperature range. All uncertainties are however, under an order of magnitude below the uncertainties found in the temperature measured by their counterparts (TC and OS) in the same range of temperature (see tables below), making these uncertainties acceptable for use in the whole range of CLOUD temperatures~~CLOUD temperature range and so are well-matched for *in-situ* calibration of the CLOUD chamber strings.

Calibration of the thermocouple, optical sensor and horizontal PT100 string

~~A CLOUD temperature calibration campaign was scheduled exclusively to calibrate the different temperature sensors in the CLOUD chamber. The campaign consisted of cycling through the different operational temperature range in CLOUD.~~ After calibrating the ~~Pt100 calibration sensors in laboratory, they were mounted in their respective strings and placed~~ calibration sensors (PTV and PTH) in the laboratory, the calibration strings were mounted inside the CLOUD chamber. Each ~~PT100 sensor in their calibration string occupies the same position of their respective calibrating string~~calibration string was built so that each calibration sensor would occupy the vertical and radial position as close as possible to the position of the sensor to be calibrated. In this way, each TC and OS sensor now had a calibrated ~~Pt100~~ sensor in close proximity ~~that was used~~ to define the calibrated temperature at that location. ~~This proximity should allow for any non-uniformities or localized events (such as condensation) in the chamber to be ignored in the calibration stage. As the strings were installed, care was taken to ensure that the sensor tips did not come into contact while also minimizing the distance between the sensor tip and it's respective Pt100 calibrating sensor tip.~~ A total of 10 experiments were ~~preformed~~ performed at temperatures ranging from -60 °C to 70 °C. Each experiment consisted of setting ~~the temperature control to the desired~~ a desired chamber temperature and acquiring data for around 24 hours. ~~No expansion measurements were made during this calibration campaign as the goal of the campaign was to find a calibration curve for all sensors in the CLOUD chamber, thus only stable temperature points were taken during this campaign.~~

To calibrate the TC and OS sensors, the difference between the temperature measured by each sensor (T_s) and ~~it's~~ its adjacent calibrated Pt100 sensor (T^*) was fitted to a polynomial:

$$T^* - T_s = \sum_{n=0}^{k_s} x_n T_s^n, \tag{A2}$$

where x_n are fitted coefficients and k_s is the degree of the polynomial fit required for each sensor. The fitted parameters ~~are then~~ were subsequently used to correct each measured sensor temperature to its calibrated value.

A least squares fit of Eq. A2 was applied to the calibrated temperature measurements for each TC sensor. A second order fit was found to best describe the data (Fig. A4a). The TC fit residuals are shown in Fig. A4b. We ~~summarize~~ summarise the fitted calibration parameters and uncertainties for the thermocouple string in Table A2. PTH2 was non responsive after being placed in the chamber. Thus ~~it's~~ its measurement was replaced by a spatial linear fit between the measurements of ~~PT1H and PT3H~~ PTH1 and PTH3 defined by:

$$T^*_{PTH2} = T_{PTH1} + (r_{PTH2} - r_{PTH1}) \frac{T_{PTH3} - T_{PTH1}}{r_{PTH3} - r_{PTH1}} \tag{A3}$$

where ~~r_{PTY} is~~ r_{PTHi} and T_{PTHi} are, respectively, the radial position ~~of sensor PTHY and T_{PTHY} is the~~ and temperature measured by ~~sensor PTHY (see table 1for details)~~the PTH sensor of index i, as defined in Table 1.

The optical sensors were calibrated in a similar way. Here a 3rd order polynomial was used, except for OS4 and OS5, which required a 4th order polynomial (Fig. A5a). OS4 displayed anomalous behavior, and to a lesser extent, also OS5. Both were calibrated ~~, but ignored from analyses~~ but ignored for analysis of the temperature uniformity in the CLOUD chamber. ~~Since replacing the sensors would require the removal of all other sensors readouts, which would affect their callibration, the sensors were not replaced.~~ The OS fit residuals are shown in Fig. A5b and are somewhat larger than those obtained for the TC sensors. We ~~summarize~~ summarise the fitted calibration parameters and uncertainties for the optical sensor string in Table A3.

The PT sensors were calibrated using a least squares fit to a linear function of the measured temperature (T_{PT}):

$$T(T_{PT}) = x_1\, T_{PT} + x_0 \tag{A4}$$

Since the ~~Pt100~~ PT string sensor positions did not contain a set of calibration sensors in their vicinity, a spatial linear interpolation of the values of the horizontal calibration string was made similar to equation A3 in order to create a virtual calibration string at the positions of the sensors in the ~~Pt100~~ PT string. The ~~P100 string is contains only~~ PT string contained originally 5 sensors~~and~~ , but PT4 ~~did not work during the period of analysis and no useful calibration or campaign data was retrieved~~was damaged prior to this study. The results of these fits are ~~summarized~~ summarised in Table A4.

Acknowledgements. This research has been supported by a Marie Curie Initial Training Network Fellowship of the European Community's Seventh Framework Programme under contract number (PITN-GA-2012-316662-CLOUD-TRAIN.)

References

Ball, S. M., Hanson, D. R., Eisele, F. L., and McMurry, P. H.: Laboratory studies of particle nucleation: Initial results for H2SO4, H2O, and NH3vapors, Journal of Geophysical Research: Atmospheres, 104, 23 709–23 718, doi:10.1029/1999jd900411, https://doi.org/10.1029/1999jd900411, 1999.

Callendar, H. L.: On the Practical Measurement of Temperature: Experiments Made at the Cavendish Laboratory, Combridge, Philosophical Transactions of the Royal Society A: Mathematical, Physical and Engineering Sciences, 178, 161–230, doi:10.1098/rsta.1887.0006, https://doi.org/10.1098%2Frsta.1887.0006, 1887.

Cocker, D. R., Flagan, R. C., and Seinfeld, J. H.: State-of-the-Art Chamber Facility for Studying Atmospheric Aerosol Chemistry, Environmental Science & Technology, 35, 2594–2601, 2001.

Commission, I. E. et al.: IEC 60751: 2008, Industrial platinum resistance thermometers and platinum temperature sensors, 2008.

Connolly, P., Emersic, C., and Field, P.: A laboratory investigation into the aggregation efficiency of small ice crystals, Atmospheric Chemistry and Physics, 12, 2055–2076, 2012.

Duplissy, J., Merikanto, J., Franchin, A., Tsagkogeorgas, G., Kangasluoma, J., Wimmer, D., Vuollekoski, H., Schobesberger, S., Lehtipalo, K., Flagan, R. C., Brus, D., Donahue, N. M., Vehkamaki, H., Almeida, J., Amorim, A., Barmet, P., Bianchi, F., Breitenlechner, M., Dunne, E. M., Guida, R., Henschel, H., Junninen, H., Kirkby, J., Kürten, A., Kupc, A., Maattanen, A., Makhmutov, V., Mathot, S., Nieminen, T., Onnela, A., Praplan, A. P., Riccobono, F., Rondo, L., Steiner, G., Tome, A., Walther, H., Baltensperger, U., Carslaw, K. S., Dommen, J., Hansel, A., Petaja, T., Sipila, M., Stratmann, F., Vrtala, A., Wagner, P. E., Worsnop, D. R., Curtius, J., and Kulmala, M.: Effect of ions on sulfuric acid-water binary particle formation: 2. Experimental data and comparison with QC-normalized classical nucleation theory, Journal of Geophysical Research: Atmospheres, 121, 1752–1775, doi:10.1002/2015JD023539, http://dx.doi.org/10.1002/2015JD023539, 2015JD023539, 2016.

Duplissy, J. et al.: Results from the CERN pilot CLOUD experiment, Atm. Chem. Phys., 10, 1635–1647, 2010.

Dusen, M. S. V.: Platinum-resistance thermometry at low temperatures, Journal of the American Chemical Society, 47, 326–332, doi:10.1021/ja01679a007, https://doi.org/10.1021%2Fja01679a007, 1925.

Gordon, H., Sengupta, K., Rap, A., Duplissy, J., Frege, C., Williamson, C., Heinritzi, M., Simon, M., Yan, C., Almeida, J., Trostl, J., Nieminen, T., Ortega, I. K., Wagner, R., Dunne, E. M., Adamov, A., Amorim, A., Bernhammer, A.-K., Bianchi, F., Breitenlechner, M., Brilke, S., Chen, X., Craven, J. S., Dias, A., Ehrhart, S., Fischer, L., Flagan, R. C., Franchin, A., Fuchs, C., Guida, R., Hakala, J., Hoyle, C. R., Jokinen, T., Junninen, H., Kangasluoma, J., Kim, J., Kirkby, J., Krapf, M., Kürten, A., Laaksonen, A., Lehtipalo, K., Makhmutov, V., Mathot, S., Molteni, U., Monks, S. A., Onnela, A., Perakyla, O., Piel, F., Petaja, T., Praplan, A. P., Pringle, K. J., Richards, N. A. D., Rissanen, M. P., Rondo, L., Sarnela, N., Schobesberger, S., Scott, C. E., Seinfeld, J. H., Sharma, S., Sipila, M., Steiner, G., Stozhkov, Y., Stratmann, F., Tome, A., Virtanen, A., Vogel, A. L., Wagner, A. C., Wagner, P. E., Weingartner, E., Wimmer, D., Winkler, P. M., Ye, P., Zhang, X., Hansel, A., Dommen, J., Donahue, N. M., Worsnop, D. R., Baltensperger, U., Kulmala, M., Curtius, J., and Carslaw, K. S.: Reduced anthropogenic aerosol radiative forcing caused by biogenic new particle formation, Proceedings of the National Academy of Sciences, 113, 12 053–12 058, doi:10.1073/pnas.1602360113, http://www.pnas.org/content/113/43/12053.abstract, 2016.

Gordon, H., Kirkby, J., Baltensperger, U., Bianchi, F., Breitenlechner, M., Curtius, J., Dias, A., Dommen, J., Donahue, N. M., Dunne, E. M., Duplissy, J., Ehrhart, S., Flagan, R. C., Frege, C., Fuchs, C., Hansel, A., Hoyle, C. R., Kulmala, M., Kürten, A., Lehtipalo, K., Makhmutov, V., Molteni, U., Rissanen, M. P., Stozkhov, Y., Tröstl, J., Tsagkogeorgas, G., Wagner, R., Williamson, C., Wimmer, D., Winkler, P. M., Yan, C., and Carslaw, K. S.: Causes and importance of new particle formation in the present-day and preindustrial atmospheres, Journal of Geophysical Research: Atmospheres, 122, 8739–8760, 2017.

Hoyle, C. R., Fuchs, C., Järvinen, E., Saathoff, H., Dias, A., El Haddad, I., Gysel, M., Coburn, S. C., Tröstl, J., Bernhammer, A.-K., Bianchi, F., Breitenlechner, M., Corbin, J. C., Craven, J., Donahue, N. M., Duplissy, J., Ehrhart, S., Frege, C., Gordon, H., Höppel, N., Heinritzi, M., Kristensen, T. B., Molteni, U., Nichman, L., Pinterich, T., Prévôt, A. S. H., Simon, M., Slowik, J. G., Steiner, G., Tomé, A., Vogel, A. L., Volkamer, R., Wagner, A. C., Wagner, R., Wexler, A. S., Williamson, C., Winkler, P. M., Yan, C., Amorim, A., Dommen, J., Curtius, J., Gallagher, M. W., Flagan, R. C., Hansel, A., Kirkby, J., Kulmala, M., Möhler, O., Stratmann, F., Worsnop, D. R., and Baltensperger, U.: Aqueous phase oxidation of sulphur dioxide by ozone in cloud droplets, Atmospheric Chemistry and Physics, 16, 1693–1712, doi:10.5194/acp-16-1693-2016, https://www.atmos-chem-phys.net/16/1693/2016/, 2016.

Huber Kältemaschinenbau AG: 77656 Offenburg, Germany, http://www.huber-online.com/en/.

Incropera, F. P. and DeWitt, D. P.: Introduction to Heat Transfer, 5th ed., Wiley, Hoboken, N.J., 2007.

Jurányi, Z., Gysel, M., Duplissy, J., Weingartner, E., Tritscher, T., Dommen, J., Henning, S., Ziese, M., Kiselev, A., Stratmann, F., George, I., and Baltensperger, U.: Influence of gas-to-particle partitioning on the hygroscopic and droplet activation behaviour of alpha-pinene secondary organic aerosol, Physical Chemistry Chemical Physics, 11, 8091, doi:10.1039/b904162a, https://doi.org/10.1039/b904162a, 2009.

Kirkby, J. et al.: Role of sulphuric acid, ammonia and galactic cosmic rays in atmospheric aerosol nucleation, Nature, 476, 429–433, 2011.

Kupc, A., Amorim, A., Curtius, J., Danielczok, A., Duplissy, J., Ehrhart, S., Walther, H., Ickes, L., Kirkby, J., Karten, A., Lima, J., Mathot, S., Minginette, P., Onnela, A., Rondo, L., and Wagner, P.: A fibre-optic UV system for H2SO4 production in aerosol chambers causing minimal thermal effects, Journal of Aerosol Science, 42, 532 – 543, doi:http://dx.doi.org/10.1016/j.jaerosci.2011.05.001, http://www.sciencedirect.com/science/article/pii/S0021850211000632, 2011.

Kürten, A., Bianchi, F., Almeida, J., Kupiainen-Maatta, O., Dunne, E. M., Duplissy, J., Williamson, C., Barmet, P., Breitenlechner, M., Dommen, J., Donahue, N. M., Flagan, R. C., Franchin, A., Gordon, H., Hakala, J., Hansel, A., Heinritzi, M., Ickes, L., Jokinen, T., Kangasluoma, J., Kim, J., Kirkby, J., Kupc, A., Lehtipalo, K., Leiminger, M., Makhmutov, V., Onnela, A., Ortega, I. K., Petaja, T., Praplan, A. P., Riccobono, F., Rissanen, M. P., Rondo, L., Schnitzhofer, R., Schobesberger, S., Smith, J. N., Steiner, G., Stozhkov, Y., Tome, A., Trostl, J., Tsagkogeorgas, G., Wagner, P. E., Wimmer, D., Ye, P., Baltensperger, U., Carslaw, K., Kulmala, M., and Curtius, J.: Experimental particle formation rates spanning tropospheric sulfuric acid and ammonia abundances, ion production rates, and temperatures, Journal of Geophysical Research: Atmospheres, 121, 12,377–12,400, doi:10.1002/2015JD023908, http://dx.doi.org/10.1002/2015JD023908, 2015JD023908, 2016.

Lovejoy, E. R.: Atmospheric ion-induced nucleation of sulfuric acid and water, Journal of Geophysical Research, 109, doi:10.1029/2003jd004460, https://doi.org/10.1029/2003jd004460, 2004.

Maahs, H. G.: Kinetics and mechanism of the oxidation of S(IV) by ozone in aqueous solution with particular reference to SO2conversion in nonurban tropospheric clouds, Journal of Geophysical Research, 88, 10 721, doi:10.1029/jc088ic15p10721, https://doi.org/10.1029/jc088ic15p10721, 1983.

Möhler, O., Stetzer, O., Schaefers, S., Linke, C., Schnaiter, M., Tiede, R., Saathoff, H., Krämer, M., Mangold, A., Budz, P., Zink, P., Schreiner, J., Mauersberger, K., Haag, W., Kärcher, B., and Schurath, U.: Experimental investigation of homogeneous freezing of sulphuric acid particles in the aerosol chamber AIDA, Atmospheric Chemistry and Physics, 3, 211–223, doi:10.5194/acp-3-211-2003, https://www.atmos-chem-phys.net/3/211/2003/, 2003.

Myhre, G., Shindell, D., Bréon, F., and Collins, W.: Anthropogenic and natural radiative forcing, Climate Change 2013: The Physical Science Basis (eds. Stocker, T.F., et al.), pp. 571–658, 2013.

National Instruments Corp.: Berkshire RG14 2PZ, United Kingdom, http://www.ni.com/en-gb.html.

Nichman, L., Fuchs, C., Järvinen, E., Ignatius, K., Höppel, N. F., Dias, A., Heinritzi, M., Simon, M., Tröstl, J., Wagner, A. C., Wagner, R., Williamson, C., Yan, C., Connolly, P. J., Dorsey, J. R., Duplissy, J., Ehrhart, S., Frege, C., Gordon, H., Hoyle, C. R., Kristensen, T. B., Steiner, G., McPherson Donahue, N., Flagan, R., Gallagher, M. W., Kirkby, J., Möhler, O., Saathoff, H., Schnaiter, M., Stratmann, F., and Tomé, A.: Phase transition observations and discrimination of small cloud particles by light polarization in expansion chamber experiments, Atmospheric Chemistry and Physics, 16, 3651–3664, doi:10.5194/acp-16-3651-2016, https://www.atmos-chem-phys.net/16/3651/2016/, 2016.

Opsens Inc.: Quebec, Canada, https://opsens.com.

Paulsen, D., Dommen, J., Kalberer, M., Prévôt, A. S. H., Richter, R., Sax, M., Steinbacher, M., Weingartner, E., and Baltensperger, U.: Secondary Organic Aerosol Formation by Irradiation of 1, 3, 5-Trimethylbenzene-NOx-H2O in a New Reaction Chamber for Atmospheric Chemistry and Physics, Environmental Science & Technology, 39, 2668–2678, doi:10.1021/es0489137, https://doi.org/10.1021/es0489137, 2005.

Raes, F. and Janssens, A.: Ion-induced aerosol formation in a H2O-H2SO4 system—II. Numerical calculations and conclusions, Journal of Aerosol Science, 17, 715–722, doi:10.1016/0021-8502(86)90051-0, https://doi.org/10.1016/0021-8502(86)90051-0, 1986.

Riechers, B., Wittbracht, F., Hütten, A., and Koop, T.: The homogeneous ice nucleation rate of water droplets produced in a microfluidic device and the role of temperature uncertainty, Physical Chemistry Chemical Physics, 15, 5873, doi:10.1039/c3cp42437e, https://doi.org/10.1039/c3cp42437e, 2013.

Schnitzhofer, R., Metzger, A., Breitenlechner, M., Jud, W., Heinritzi, M., De Menezes, L.-P., Duplissy, J., Guida, R., Haider, S., Kirkby, J., Mathot, S., Minginette, P., Onnela, A., Walther, H., Wasem, A., and Hansel, A.: Characterisation of organic contaminants in the CLOUD chamber at CERN, Atmospheric Measurement Techniques, 7, 2159–2168, doi:10.5194/amt-7-2159-2014, https://www.atmos-meas-tech.net/7/2159/2014/, 2014.

Suller, V. P. and Petit-Jean-Genaz, C., eds.: EPAC 94. Proceedings, 4th European Particle Accelerator Conference, London, UK, June 27 - July 1, 1994. Vol. 1-3, 1995.

Voigtlander, J., Duplissy, J., Rondo, L., Kürten, A., and Stratmann, F.: Numerical simulations of mixing conditions and aerosol dynamics in the CERN CLOUD chamber, Atmospheric Chemistry and Physics, 12, 2205–2214, doi:10.5194/acp-12-2205-2012, http://www.atmos-chem-phys.net/12/2205/2012/, 2012.

WIKA Alexander Wiegand SE & Co. KG: 63911 Klingenberg, Germany, http://en-co.wika.de/home_en_co.WIKA.

Wilson, C. T. R. and Wilson, J. G.: On the Falling Cloud-Chamber and on a Radial-Expansion Chamber, Proceedings of the Royal Society A: Mathematical, Physical and Engineering Sciences, 148, 523–533, doi:10.1098/rspa.1935.0032, https://doi.org/10.1098/rspa.1935.0032, 1935.

Zink, P.: Cryo-chamber simulation of stratospheric H2SO4/H2O particles: Composition analysis and model comparison, Geophysical Research Letters, 29, doi:10.1029/2001gl013296, https://doi.org/10.1029/2001gl013296, 2002.

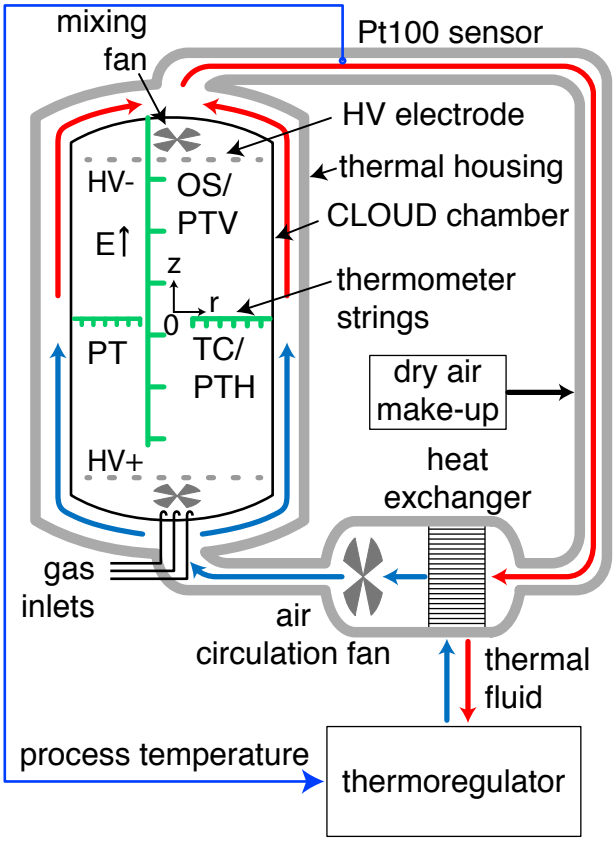

Figure 1. Schematic of the CLOUD thermal system. Thermally-controlled air is circulated by a fan at a rate of around 7200 m^3/h within a thermally-insulated housing surrounding the stainless steel CLOUD chamber (3 m diameter, 26.1 m^3 volume). The air is returned to the bottom of the chamber along an insulated duct, where it passes through a heat exchanger. A small flow of desiccated air is added to compensate for leaks and ensure that the dew point of the re-circulated air remains well below -80 °C. The air is precisely maintained at a selectable "process temperature" in the range between -70 °C and +100 °C by a 36 kW thermoregulator (Unistat 850W; Huber Kältemaschinenbau AG) which controls the temperature of thermal fluid circulating through the heat exchanger. Fresh make-up air and trace gases continuously enter the chamber to compensate for sampling losses and maintain 5 mbar over-pressure inside the chamber. The chamber air is injected underneath the lower mixing fan (z=0 m) at rates between 20 l/min (during sensor calibration) and 210 l/min (during CLOUD campaigns). During data campaigns, vertical electrical fields of up 20 kV/m are generated inside the CLOUD chamber by a pair of HV electrodes whose mid-plane (at 0 V potential) coincides with the mid plane of the chamber. The temperature of the air inside the CLOUD chamber is measured by several precision thermometer strings, indicated by green lines. ~~On origin axis is presented~~ The *r z* cylindrical coordinate axes are indicated in the figure~~to guide~~, with the ~~user~~ origin in ~~determining~~ the ~~position~~ centre of the ~~sensors in the~~ chamber~~via table~~, as a guide for the sensor positions indicated in Table 1

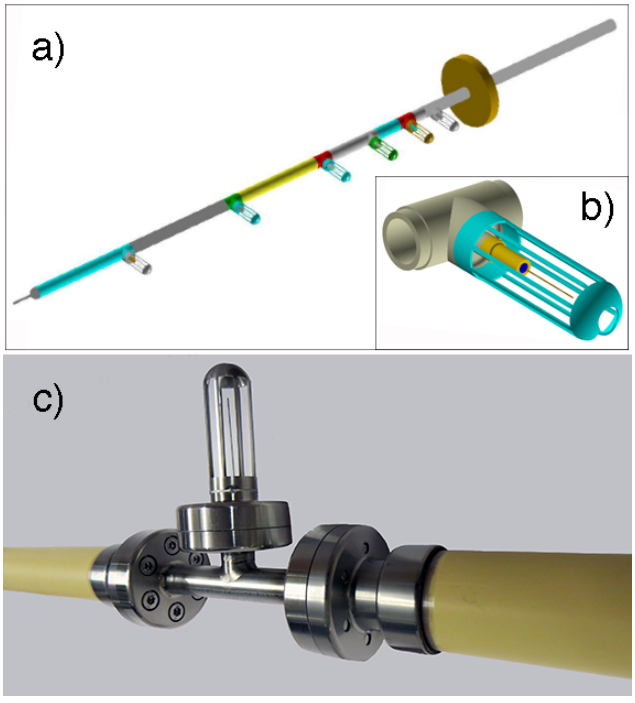

Figure 2. Images of two temperature strings showing a) a model drawing of the thermocouple (TC) string with 6 TC sensors and one Pt100 sensor at the tip, mounted on a 1.25 m stainless steel support tube welded to a DN100 flange, b) a model drawing of a single TC sensor (thin brown line), and c) a photograph of an approximately 25 cm section of the optical sensor string showing a sensor mounted inside a stainless steel capillary and transition structure that is welded to two partially-conducting zirconia ceramic tube spacers of 27 mm outer diameter (yellow). The sensors are mounted inside Faraday cages (e.g. coloured blue in panel b) to protect against corona discharge when a 20 kV/cm vertical electric field is present in the CLOUD chamber. Ultra-clean materials (stainless steel and ceramics) are used throughout, with the readout wires/optical fibers passing inside the hollow support structures.

Table 1. Position of the temperature sensors in CLOUD. The CLOUD chamber is a cylinder of 150 cm radius (r) and approximately 400 cm height (z). The origin of the cylindrical coordinate system is located in the centre of the chamber, with the z axis pointing vertically upwards (Fig. 1). The ~~Pt100~~ calibration strings, PTH and PTV, have Pt100 sensor locations that ~~closely match those~~ are located within about 1 cm of the indicated sensor locations for the TC and OS strings, respectively. The calibration strings, which are only installed during calibration measurements, are displaced laterally from the TC string by Δz = -20 cm (PTH) and from the OS string by 10 cm azimuthally (PTV).

	Horizontal strings: Thermocouple (TC) and Calibration (PTH; $\pm$1 cm)		Vertical strings: Optical (OS) and Calibration (PTV; $\pm$1 cm)		Horizontal string: Pt100 (PT)	
Sensor #	Radius, r ~~(cm)~~ (cm)	Height, z ~~(cm)~~ (cm)	Radius, r ~~(cm)~~ (cm)	Height, z ~~(cm)~~ (cm)	Radius, r ~~(cm)~~ (cm)	Height, z (cm)
1	145 ~~(PTH $\pm$ 1)~~	0	50	123.1 ~~(PTV $\pm$ 1)~~	145	0
2	138 ~~(PTH $\pm$ 1)~~	0	50	78.3 ~~(PTV $\pm$ 1)~~	115	0
3	128 ~~(PTH $\pm$ 1)~~	0	50	33.5 ~~(PTV $\pm$ 1)~~	90	0
4	115 ~~(PTH $\pm$ 1)~~	0	50	-11.3 ~~(PTV $\pm$ 1)~~	-	-
5	90 ~~(PTH $\pm$ 1)~~	0	50	-56.1 ~~(PTV $\pm$ 1)~~	60	0
6	60 ~~(PTH $\pm$ 1)~~	0	50	-100.9 ~~(PTV $\pm$ 1)~~	-	-

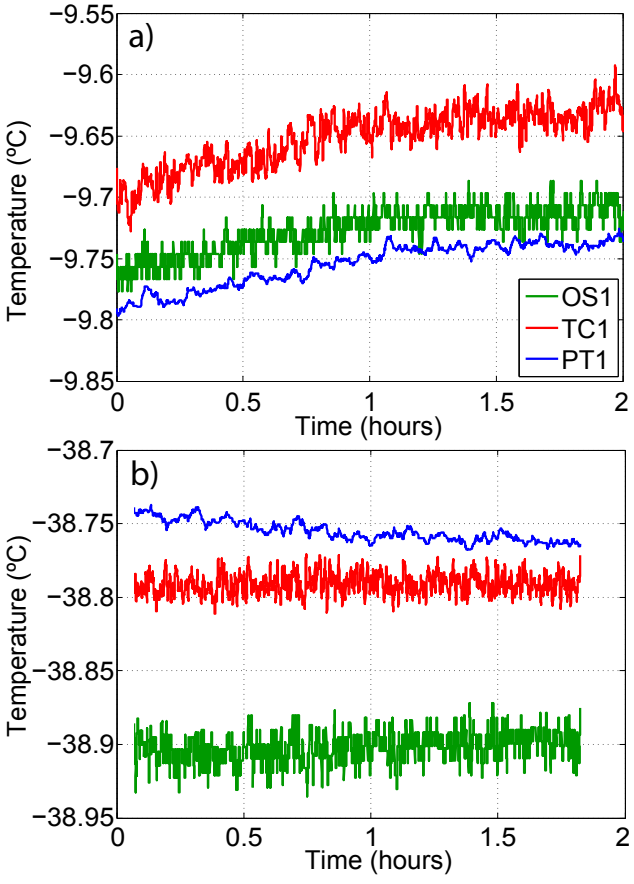

Figure 3. Examples of the typical temperature stability in the CLOUD chamber over a period of several hours: a) during an experimental data run and b) during a calibration run (OS, optical sensor; TC, thermocouple, TC; and PT, Pt100 sensor). The temperature drift in panel a) can result from setting new experimental conditions such as the addition of ultra violet radiation or trace gases, which causes a slight change in equilibrium temperature. The measurements are smoothed with a ~~15~~ 5 s fixed median window ~~firstly~~ to ~~improve the measurement result by removing any outlier values of the measurement distribution and secondly to improve readability of the figure by the reader~~reduce point-to-point scatter.

Table 2. ~~Table of the CLOUD campaign experiments used~~ Experiments selected to ~~characterize~~ characterise the chamber ~~'s nucleation experiments~~temperature uniformity during the CLOUD9 campaign. ~~These~~ The experiments were ~~chosen due~~ selected to ~~being experiments that required stable conditions and~~ have 3-hour periods at various temperatures during which no changes ~~made to~~ of the ~~different parameters used. Between experiments, several~~ gas or other conditions ~~vary such as sulfuric acid concentration but only the parameters that are suspected of affecting the temperature distribution are displayed~~were made.

~~Experiment~~ Date of experiment	Temperature ~~Set point (~~ (°C)	Fan speed ~~Fan speed~~ (%)	Duration ~~Duration~~ (min)
29 September 2014	-10	21	185
8 October 2014	-30	21	180
25 October 2014	-10	100	180
26 October 2014	-20	100	180
27 October 2014	-20	21	180
29 October ~~1~~ 2014	-40	100	180
29 October ~~2~~ 2014	-40	21	180

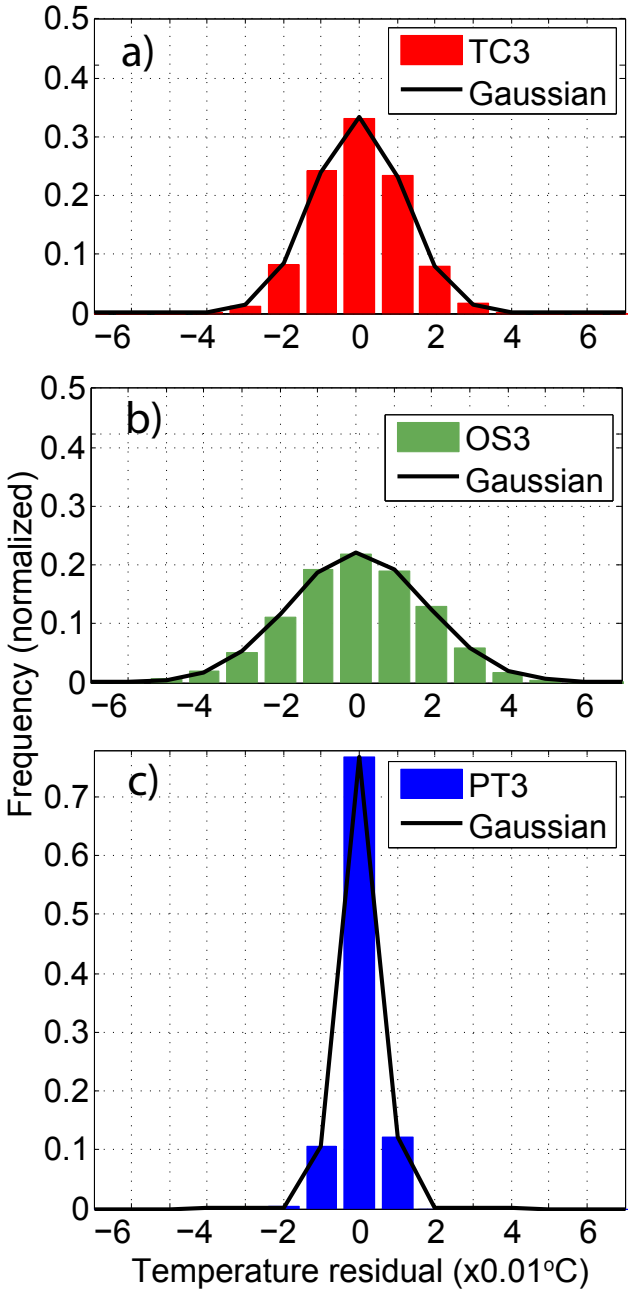

Figure 4. ~~Temperature~~ Examples of the characteristic temperature residuals from their mean values over periods of several hours during calibration runs for a) TC3 at -40 °C, b) OS3 at -0 °C and c) PT3 at -30 °C. ~~The~~ Slow trends in the data have been removed, and the measurements are smoothed with a ~~15~~ 5 s fixed median window~~for the reasons specified in figure 3, and slow trends in the data have been removed~~. The standard deviations of Gaussian fits to the data are a) 0.012 °C, b) 0.018 °C, and c) 0.004 °C. ~~OS3, TC3 and PT3 were chosen due to being the central sensors~~ See supplement material for distributions of ~~each respective string~~other sensors.~~The temperatures chosen represent common temperatures used during CLOUD campaigns.~~

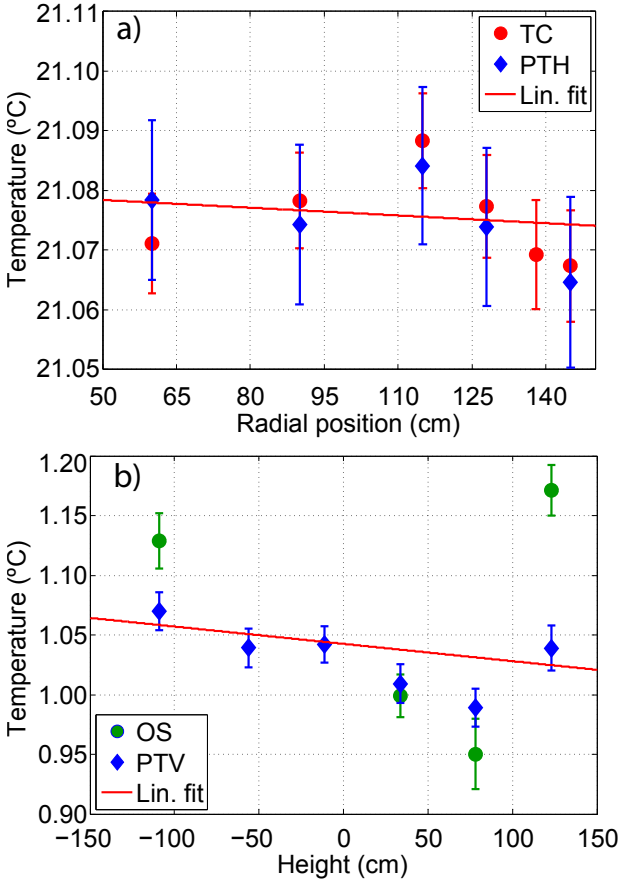

Figure 5. Comparison of the temperature non-uniformity measured by several sensor strings in a) the radial and b) the vertical directions during calibration runs at 21 °C and 1 °C, respectively. Linear fits are shown to guide the eye. OS4 and OS5 are not included in panel b (see Appendix A for details). The error bars in this and other figures show 1 sigma statistical uncertainties and do not account for possible systematic uncertainties.

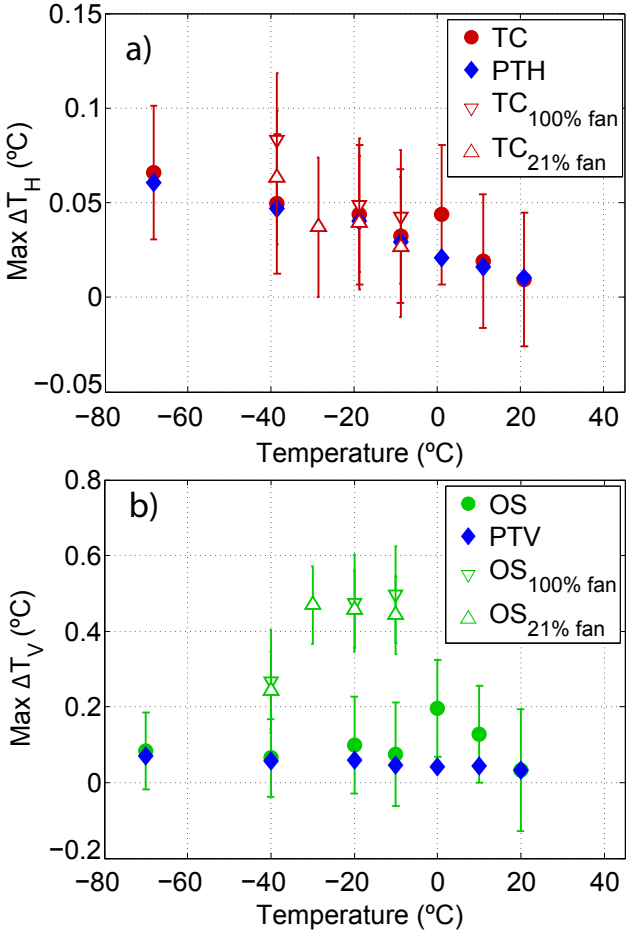

Figure 6. Maximum temperature difference from the string mean (temperature non-uniformity), ΔT, in the a) horizontal and b) vertical directions at chamber temperatures between -70 °C and 20 °C. The data were recorded during both calibration (~~filled~~solid symbols) and data-taking runs (hollow symbols) in June and ~~November~~ September–October 2014, respectively.~~During the campaign of November 2014, periods with the same temperature and different fan operating speeds (84 and 400 rpm, 21% and 100% respectively) were recorded.~~

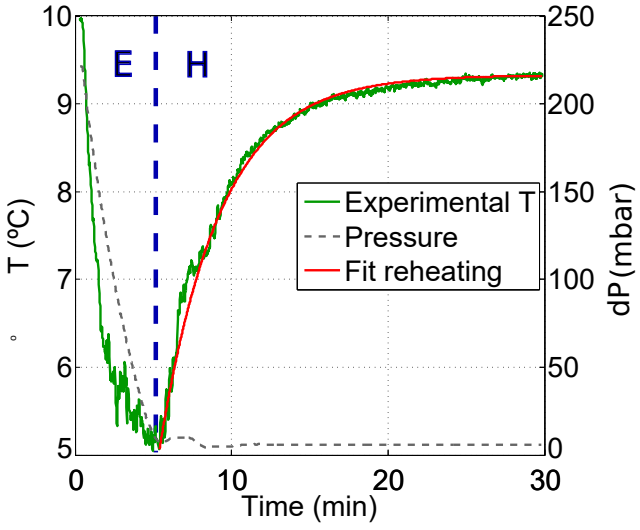

Figure 7. Example of an adiabatic pressure reduction to form a cloud in the CLOUD chamber. The chamber pressure is reduced from 220 mbar to 5 mbar above one atmosphere pressure during a period of 5 minutes (dashed curve and right-hand scale). This produces of reduction of the air temperature by around 5 °C (green curve and left-hand scale, recorded by a TC sensor). Provided the initial relative humidity is sufficiently high, a liquid cloud forms in the chamber during the cool period. The air in the chamber then returns to its equilibrium temperature set by the relatively warm chamber walls, and the cloud eventually evaporates. In this example the initial air temperature, before expansion, had not yet reached the equilibrium value near 9.3 °C. The red line is an exponential fit to the warming period with a time constant of 200 s (Eq. 1).

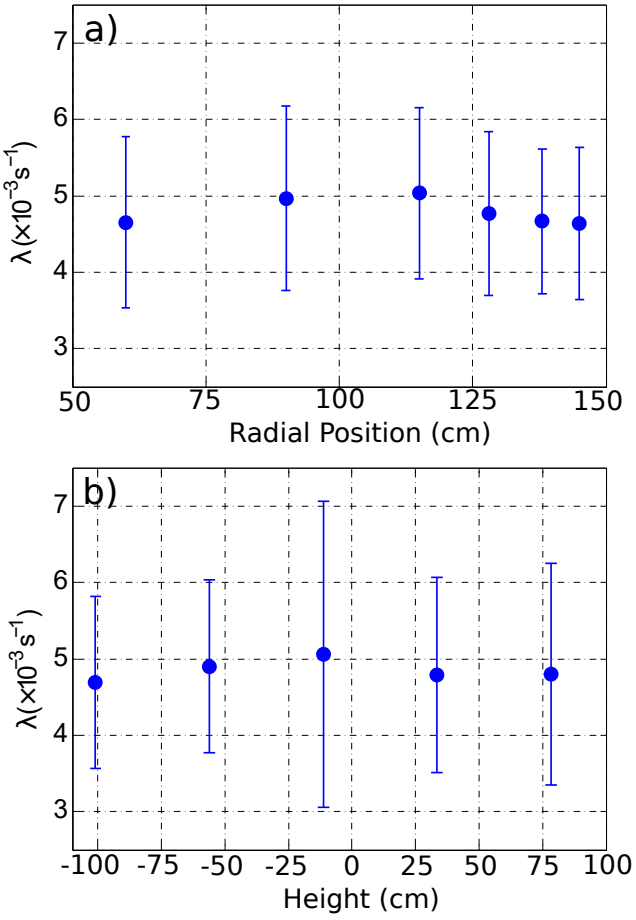

Figure 8. Air reheating rates (λ) following an adiabatic pressure reduction versus a) radial and b) vertical position in the chamber. The data points show the mean and standard deviations of the air reheating rates obtained for 300 expansions in the CLOUD9 campaign.

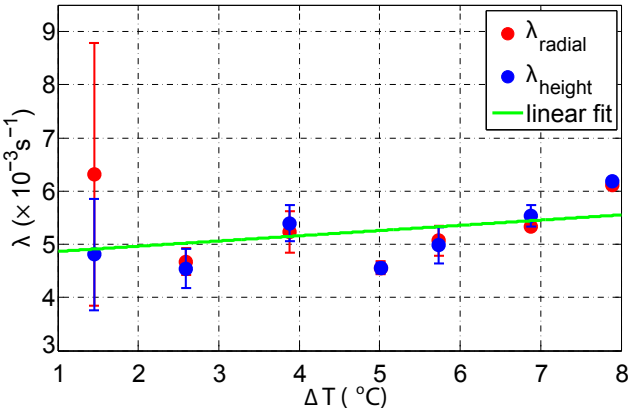

Figure 9. Air reheating rates (λ) following an adiabatic pressure reduction versus the initial temperature reduction.

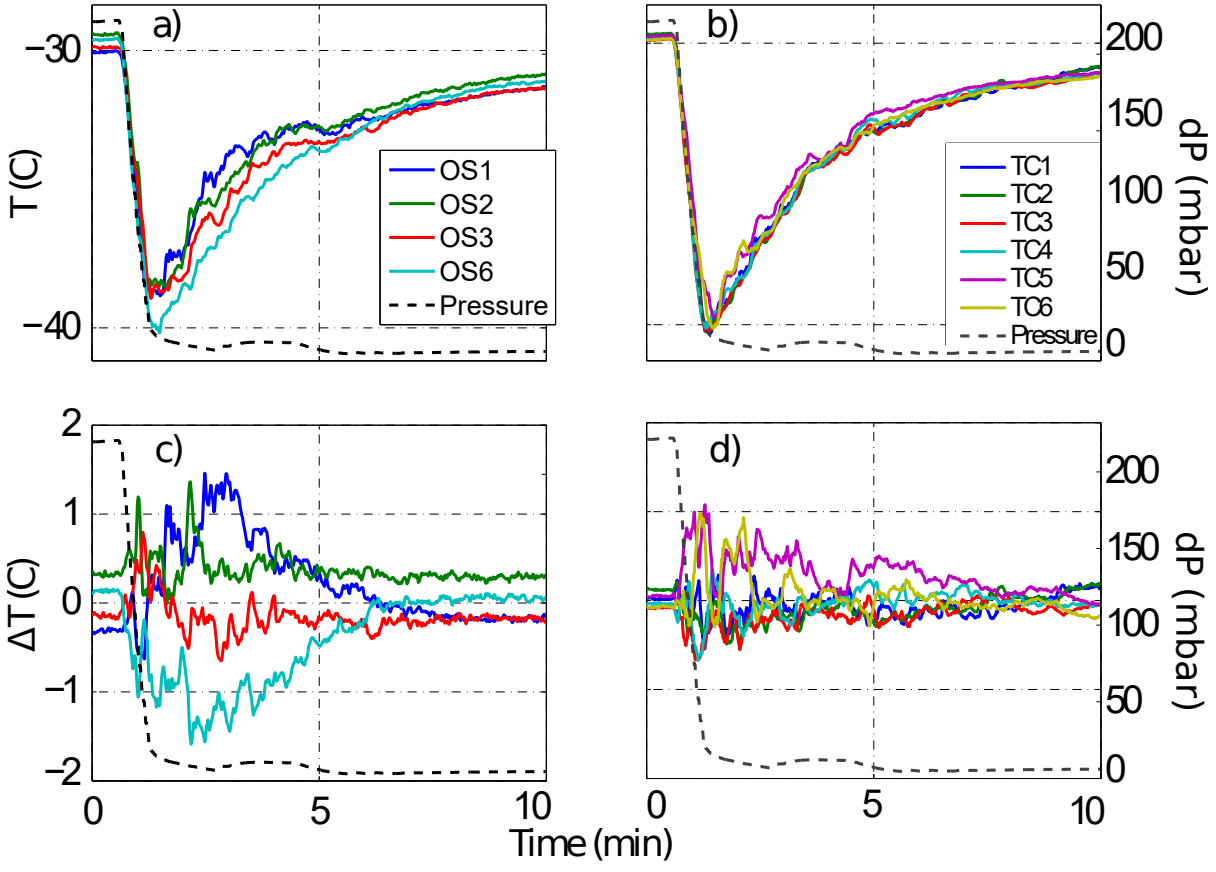

Figure 10. Temperature non-uniformities following an adiabatic pressure reduction during CLOUD9 at -30 °C in a) the vertical direction (OS) and b) the horizontal direction (TC). Panels c and d show the residuals from the mean temperatures in the vertical and horizontal directions, respectively. The relative air pressures are shown by dashed curves. Compared with operation under equilibrium conditions (Fig. 6), larger non-uniformities of up to ~~around ±1.0~~1.5 °C in the vertical direction and ±1 °C in the horizontal direction are present ~~at~~ while the ~~minimum~~ chamber returns to its equilibrium temperature ~~during adiabatic pressure reductions~~with time constant of about 200 s.

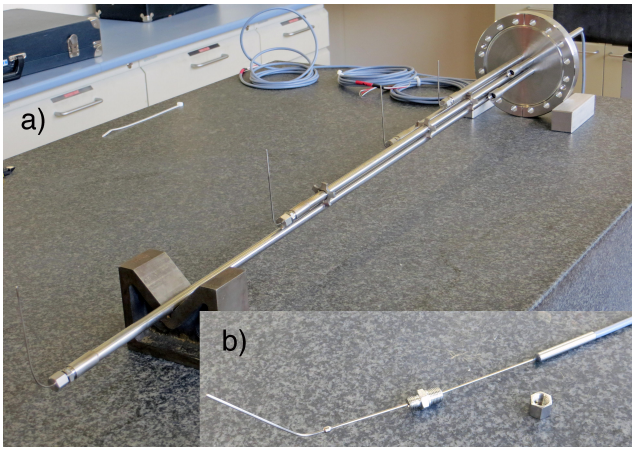

Figure A1. The horizontal ~~Pt100~~ calibration string (PTH) showing a) the string during assembly, with 4 of the 6 Pt100 sensors mounted and b) a single Pt100 sensor before mounting in the string (a 1.5 mm diameter stainless steel sheath surrounds the actual Pt100 sensor). The ~~Pt100~~ calibration strings are designed to allow the sensors to be dismounted without ~~disconnecting~~ disconnection from their readout electronics.

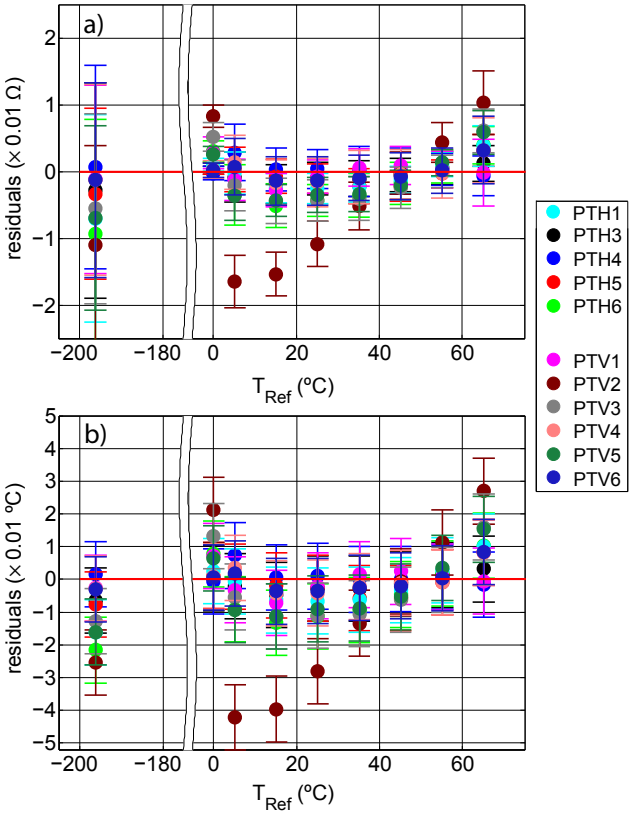

Figure A2. Residuals of the least squares fits to the CVD equation (Eq. A1 and Table A1), for the horizontal (PTH) and vertical (PTV) ~~Pt100~~ calibration strings versus temperature: a) resistance residuals and b) temperature residuals. The data were obtained during the laboratory calibration, July 2014.

Table A1. Fitted parameters and one standard deviation uncertainties of the Callendar-van-Dusen (CVD) coefficients (Eq. A1) for the horizontal and vertical ~~Pt100~~ calibration strings, PTH and PTV, obtained during the laboratory calibration, July 2014. The parameter C was fixed at $-4.183 \times 10^{-12}\ \Omega\ ^{\circ}C^{-3}$.

	R_0^{fit}	σR_0	A^{fit}	σA	B^{fit}	σB	Fit R^2
PTH1	100.0322	9.36E-4	3.908E-3	3.25E-07	-6.62E-07	3.70E-09	0.9991
PTH3	100.0216	2.55E-4	3.908E-3	1.27E-07	-6.70E-07	1.55E-09	0.9998
PTH4	99.98723	3.06E-4	3.914E-3	1.03E-07	-6.54E-07	1.06E-09	0.9999
PTH5	100.0453	6.86E-4	3.907E-3	2.26E-07	-6.60E-07	2.35E-09	0.9995
PTH6	100.0182	1.98E-3	3.913E-3	5.80E-07	-6.46E-07	5.80E-09	0.9982
PTV1	100.0496	1.11E-3	3.910E-3	3.17E-07	-6.61E-07	2.52E-09	0.9996
PTV2	100.0364	5.26E-3	3.908E-3	1.59E-06	-6.87E-07	1.35E-08	0.9894
PTV3	100.0503	2.61E-3	3.909E-3	6.64E-07	-6.69E-07	5.46E-09	0.9981
PTV4	100.0355	5.17E-4	3.912E-3	1.81E-07	-6.49E-07	1.52E-09	0.9999
PTV5	100.0184	1.79E-3	3.910E-3	5.32E-07	-6.80E-07	5.19E-09	0.9979
PTV6	100.0108	3.91E-4	3.912E-3	1.51E-07	-6.48E-07	1.37E-09	0.9999

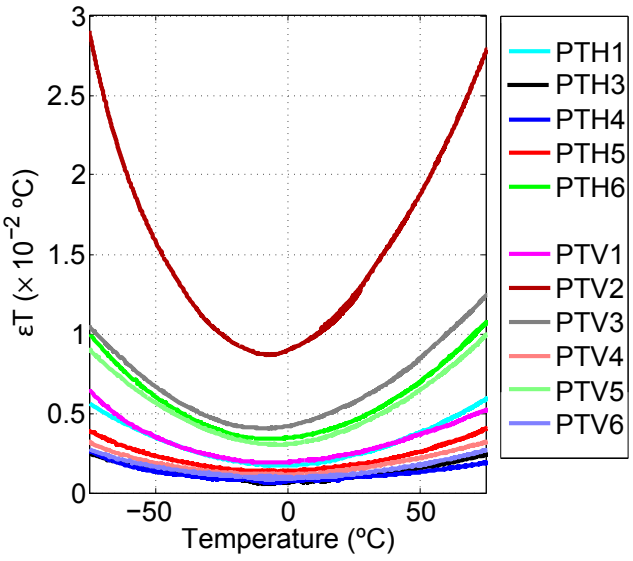

Figure A3. Estimated uncertainty of the temperature measurement of each ~~Pt100~~ calibration sensor versus temperature, based on the individual fits of the laboratory calibration measurements to the CVD equation. After calibration, almost all sensors have an uncertainty below 0.01 °C over the indicated temperature range.

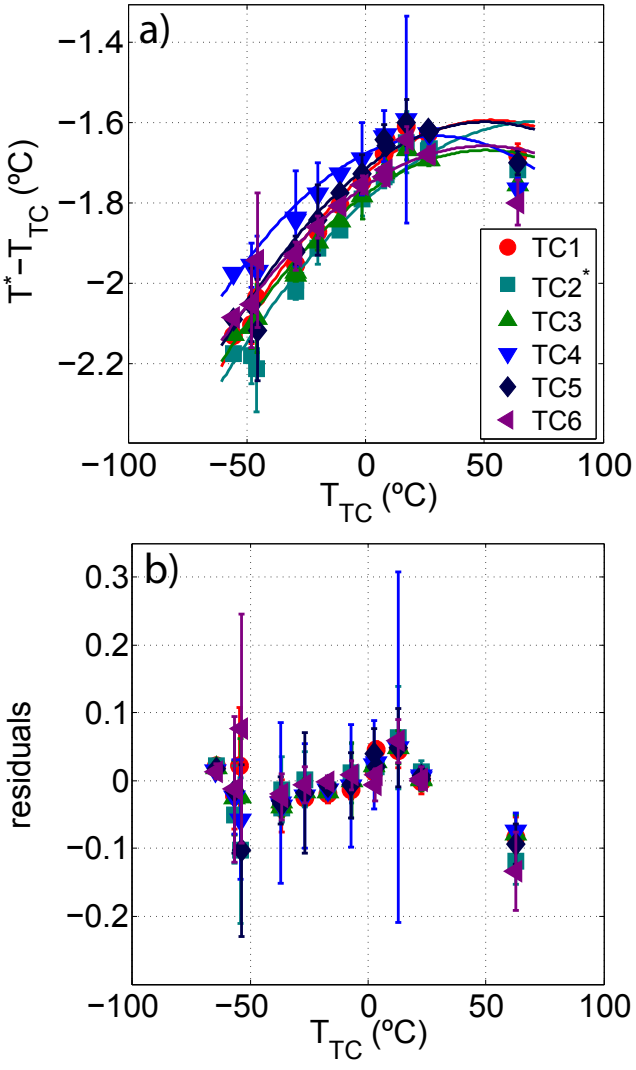

Figure A4. Calibration of the TC string during during the CLOUD calibration campaign: a) fitted calibration curves (Eq. A2 with $k_s = 2$) and b) residuals from the calibration fit. There was a malfunction of the Pt100 sensor (PTH2) for TC2 so the PTH2 values were obtained by interpolation between PTH1 and PTH3.

Table A2. Fitted calibration parameters and one standard deviation uncertainties for the thermocouple string obtained during the CLOUD calibration campaign.

Sensor	x_2	σx_2	x_1	σx_1	x_0	σx_0	χ^2/ν
TC1	-6.39E-5	1.28E-5	4.47E-2	4.40E-04	-1.70	1.50E-02	0.34
TC2	-6.04E-5	1.36E-5	4.27E-2	7.74E-04	-1.74	1.70E-02	0.44
TC3	-6.17E-5	1.01E-5	3.85E-2	3.46E-04	-1.75	1.20E-02	0.25
TC4	-6.39E-5	1.56E-5	2.35E-2	1.10E-03	-1.66	1.80E-02	0.71
TC5	-6.55E-5	2.17E-5	4.01E-2	7.23E-04	-1.68	2.50E-02	1.41
TC6	-6.51E-5	1.31E-5	2.93E-2	4.45E-04	-1.72	1.60E-02	0.46

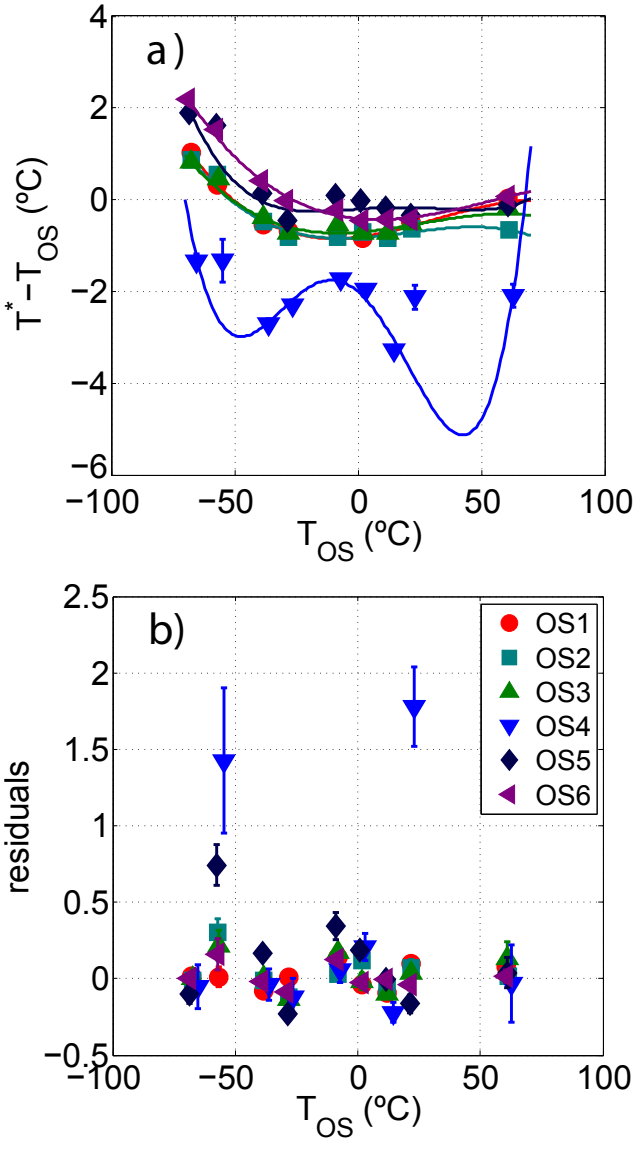

Figure A5. Calibration of the OS string during during the CLOUD calibration campaign: a) fitted calibration curves (Eq. A2 with $k_s = 3$ or 4) and b) residuals from the calibration fit.

Table A3. Fitted calibration parameters and one standard deviation uncertainties for the optical sensor string obtained during the calibration campaign.

Sensor	x_4	σx_4	x_3	σx_3	x_2	σx_2	x_1	σx_1	x_0	σx_0	χ^2/ν
OS1	N/A	N/A	-3.81E-6	2.93E-6	2.68E-4	1.48E-4	9.60E-3	9.30E-3	-7.42E-1	2.01E-1	28.40
OS2	N/A	N/A	-4.35E-6	1.97E-6	1.75E-4	8.66E-5	7.34E-3	6.60E-3	-7.65E-1	1.33E-1	7.02
OS3	N/A	N/A	-2.89E-6	2.23E-6	2.30E-4	1.04E-4	5.74E-3	7.10E-3	-7.22E-1	1.86E-1	12.34
OS4	2.54E-7	2.52E-7	-1.01E-6	8.71E-6	-1.04E-3	1.00E-3	1.12E-3	2.76E-2	-1.74	0.46	4.67
OS5	1.36E-7	3.48E-7	-1.09E-6	1.23E-5	3.77E-4	1.50E-3	5.27E-3	3.89E-2	-3.25E-2	6.97E-1	45.72
OS6	N/A	N/A	-2.16E-6	2.66E-6	3.27E-4	1.27E-4	4.64E-3	7.50E-3	-408E-1	1.74E-1	19.32

Table A4. Fitted calibration parameters and one standard deviation uncertainties for the Pt100 string during the calibration campaign.

	x_0	σx_0	x_1	σx_1	Fit R^2
PT1	0.561	0.020	1.011	0.001	1.00
PT2	0.187	0.083	1.012	0.002	1.00
PT3	0.453	0.020	1.007	0.001	1.00
PT5	0.335	0.025	0.998	0.001	1.00